

Student Development of a Liquid Oxygen, Liquid Methane Sounding Rocket and Launch Infrastructure

Silas A. Meriam*, Christopher Nilsen†, Matthew A. Tanner ‡, Kyle Runkle§, Jacob Bartkiewicz¶, Robert Groome||, and Scott Meyer**

Purdue University, West Lafayette, Indiana, 47906

Since January 2017, students at Purdue University have been developing a liquid oxygen, liquid methane sounding rocket according to the competition guidelines of the Friends of Amateur Rocketry and Mars Society launch competition. The rocket was designed, manufactured, and tested by student members of Students of the Exploration and Development of Space (SEDS) with assistance in manufacturing of more complex parts coming from key partners. The vehicle underwent component design, system design, and test readiness reviews and was tested at each of those levels over a two and a half year period. The following paper is a final report on this system, documenting both the processes taken to complete the project and the important lessons learned along the way.

I. Nomenclature

Variables

\dot{Q}	= Volumetric Flow Rate
η	= Efficiency
σ	= Stress
ε	= Expansion ratio
A_t	= Throat area
c	= Constant factor
C^*	= Characteristic velocity
C_d	= Discharge coefficient
C_f	= Thrust coefficient
C_r	= Contraction ratio
C_v	= Valve flow coefficient
d	= Diameter
D_H	= Hydraulic diameter
E	= Young's modulus
F	= Thrust
f_d	= Friction factor
G	= Specific gravity
g_0	= Acceleration due to gravity
I	= Moment of Inertia
I_{sp}	= Specific impulse
L	= Length

L^*	= Characteristic length	<i>in</i>
GPM	= Mass	<i>lb_m</i>
O/F	= Mixture ratio	
psi	= Pressure	<i>psi_a</i>
P		
r_t	= Throat radius	<i>in</i>
in^2	= Density	<i>lb_m/ft³</i>
rho		
t	= Time	<i>s</i>
ft/s	= Velocity	<i>ft/s</i>
u		
V	= Volume	<i>in³</i>
Acronyms		
CEA	= Chemical Equilibrium with Applications	
DAQ	= Data Acquisition and Control	
EDX	= Energy Dispersive X-Ray	
FOD	= Foreign Object Debris	
GHe	= Gaseous Helium	
$GLOW$	= Gross Lift-Off Weight	
$LCH4$	= Liquid Methane	
LOX	= Liquid Oxygen	
$P&ID$	= Plumbing and Instrumentation Diagram	
in^4	= Pressure transducer	
PT		
s	= Thermocouple	
TC		
in	= Direct current voltage	
VDC		

*Lead Engineer, MSci '19, Chaffee Hall, 500 Allison Road, West Lafayette, Indiana

†Program Manager, BSci '19, Chaffee Hall, 500 Allison Road, West Lafayette, Indiana

‡Propulsion Lead, MSci '18, Chaffee Hall, 500 Allison Road, West Lafayette, Indiana

§Ground Support Lead, BSci '19, Chaffee Hall, 500 Allison Road, West Lafayette, Indiana

¶Controls Lead, BSci '20 Chaffee Hall, 500 Allison Road, West Lafayette, Indiana

||Manufacturing Lead, BSci '19 Chaffee Hall, 500 Allison Road, West Lafayette, Indiana

**Lab Managing Director and Project Advisor, Maurice J. Zucrow Labs, 500 Allison Road, West Lafayette, Indiana

II. Introduction

PURDUE University has a long and celebrated history of research and development of propulsion systems which lent heavily to the development of the systems contained within this paper. From 2010 through 2013, design classes and full time researchers developed the infrastructure and technical experience required to test liquid methane and liquid oxygen rocket engines at the $5,000 \text{ lb}_f$ level.[1] This infrastructure and technical experience was instrumental to the 2017-2019 liquid team as they began development of boilerplate hardware, eventually leading to buildup and testing on Zucrow Lab's "10K" stand. Other work was conducted from 2004 through 2013 to develop a hybrid launch vehicle and ground support equipment.[2][3] This hardware went through several iterations and proved useful to a number of classes, researchers, and industry partners. Specifically, the hybrid rocket team made several key design choices that were utilized and improved upon in the design and development of the 2017-2019 liquid rocket. Key techniques were copied that lead to reduced requirements on high risk and complex components, such as run valve actuators and quick disconnects.

The 2017 announcement of a student liquid rocket competition by the Friends of Amateur Rocketry and the MARS Society inspired Purdue University faculty, staff, and students to once again eagerly pursue the development of liquid propulsion systems at the undergraduate level. The Purdue chapter of the Students for the Exploration and Development of Space began design work in the Spring of 2017 on a liquid methane, liquid oxygen sounding rocket and the associated ground support equipment required to remotely complete fill and launch operations.

III. Requirements Overview

The requirements set upon the vehicle followed from the FAR-MARS competition requirements issued in Spring 2017.[4] The top level requirements call for a bi-propellant liquid rocket capable of reaching at least 30,000 feet with a maximum total impulse of $9,206 \text{ lb}_f \text{ s}$. The team closest to 45,000 feet at the end of the annual competition window has a chance to take home \$50,000. A secondary prize, also of \$50,000, is offered to the team that meets the criteria of the first using liquid oxygen and liquid methane. The system was required to have remote data acquisition and control, with no manual pull cables or visual inspection of gauges. From these competition specifications, the following requirements were established for the Purdue vehicle:

- The rocket shall have a GLOW of 125 lb_m or less
- The propulsion system shall produce 1125 lb_f of thrust for a total duration of 8.1 seconds
- The propulsion system shall utilize liquid oxygen and liquid methane for propellants
- The propulsion system shall be pressure fed by a gaseous helium tank
- The engine shall utilize a pintle injector and an ablative chamber
- The vehicle shall have a dual deployment parachute recovery system
- The ground support system and rocket shall be remotely operated and launched for all hazardous operations
- The ground support system shall provide liquid methane and liquid oxygen to the vehicle at -260°F or colder

These requirements were derived from a need for rapid development and manufacturing. At the time of design, there was approximately a year and a half to design, build, test, and fly the system in order to meet the competition deadlines. Additional requirements were set for the design and fabrication of a test vehicle, including the development a boilerplate injector and chamber to verify injector design characteristics.

IV. Design Overview

The Purdue Liquid Methane, Liquid Oxygen Sounding Rocket is a fifteen foot tall, 120 lb GLOW sounding rocket. The vehicle is segmented into a propulsion system which consists of the tankage, plumbing, engine, and supporting structure, all of which are contained in the first 10 feet of rocket. The remaining five feet contain the recovery system, the tracking system, and optional room for a small payload. The system design, with the exception of the propulsion system, was outlined in the team's SciTech paper from earlier this year and provides a more general overview of the system.[5] The launch infrastructure consists of a 22 foot trailer that supports the the data acquisition and control system and the fluid components for filling and venting the rocket. It also supports the 30 foot launch rail and transport of the rocket to the launch site. The nearly complete system is pictured in Figure 1, which includes all of the major ground support equipment assemblies, the launch rail, and the rocket.



(a)

(b)

Fig. 1 (a) The rocket and (b) rocket and ground support system pictured vertical on July 20th, 2019.

A. Propulsion System Overview

The propulsion system on the Purdue Liquid Methane, Liquid Oxygen Sounding Rocket is designed for a total mass flow rate of $4.1 \text{ lb}_m/\text{s}$ and a chamber pressure of 550 psia , resulting in a total design thrust of just over 1100 lb_f . The plumbing and instrumentation diagram (P&ID) for the rocket's propulsion system is presented in the Appendix in Figure 25. The key features of this system are an ablative chamber, a pintle injector, bonnetless cryogenic run valves, and coaxial tanks.

The ablative chamber, pictured in Figure 2, was designed by students in conjunction with Mr. Dan Moser of Compositex Inc. An ablative chamber was chosen to minimize engine complexity and reduce system weight. The engine consists of a silica-phenolic composite liner that is shaped on a mold and inserted into an aluminum flange. The flange and liner are then joined using a carbon fiber over-wrap that also serves as the pressure vessel. The chamber has a contraction ratio of 8 and an expansion ratio of 6.7. The expansion ratio was selected based on modeling of the trajectory, where the time the rocket spent at given altitude was weighted and then the mean altitude was selected as the optimum expansion target.

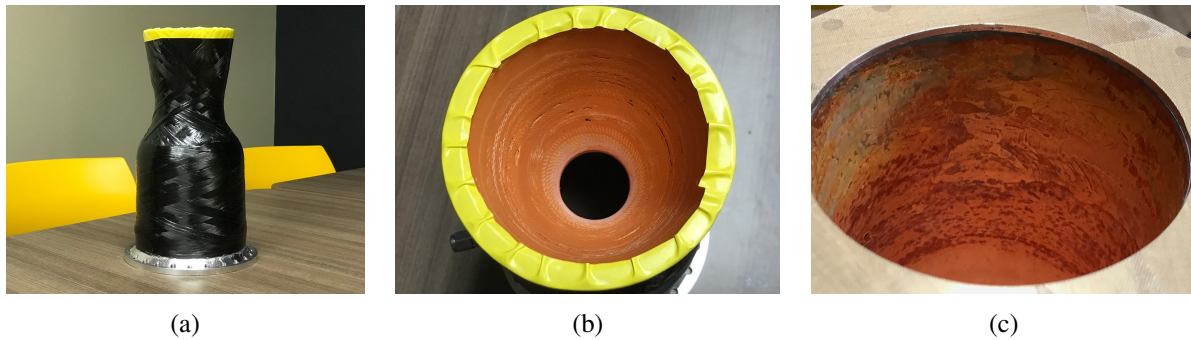


Fig. 2 From left to right: Chamber assembly, inside of the nozzle, and inside of the chamber

A pintle injector was selected early into the process due to the availability of literature and the desire to minimize combustion instabilities, instead of improving combustion efficiency. The resulting design is a fuel-centered pintle with a ΔP of 20% across the entire injector. The oxygen manifold is fed by two inlet points, each separated by 180 degrees. The injector underwent two iterations: an all stainless steel 2-piece boilerplate version and then a 3-piece stainless and

aluminum flight weight version, pictured in Figure 3. For the flight weight version of the engine, the injector used a three piece design over the test model's two pieces, which reduced the components mass by roughly 4 pounds.



Fig. 3 (a) The boilerplate injector assembly and (b) the flight weight injector assembly

The complete engine assembly is presented in an exploded view and in its final assembly in Figure 4. The engine design changed slightly from critical design review in Fall 2017 to the time the final engine was fabricated. These changes are reflected in the differences between Figure 4a and Figure 4b. The engine gained a bell curve and reduced mass by removing material from the exterior wrapping and modifications to the injector design.

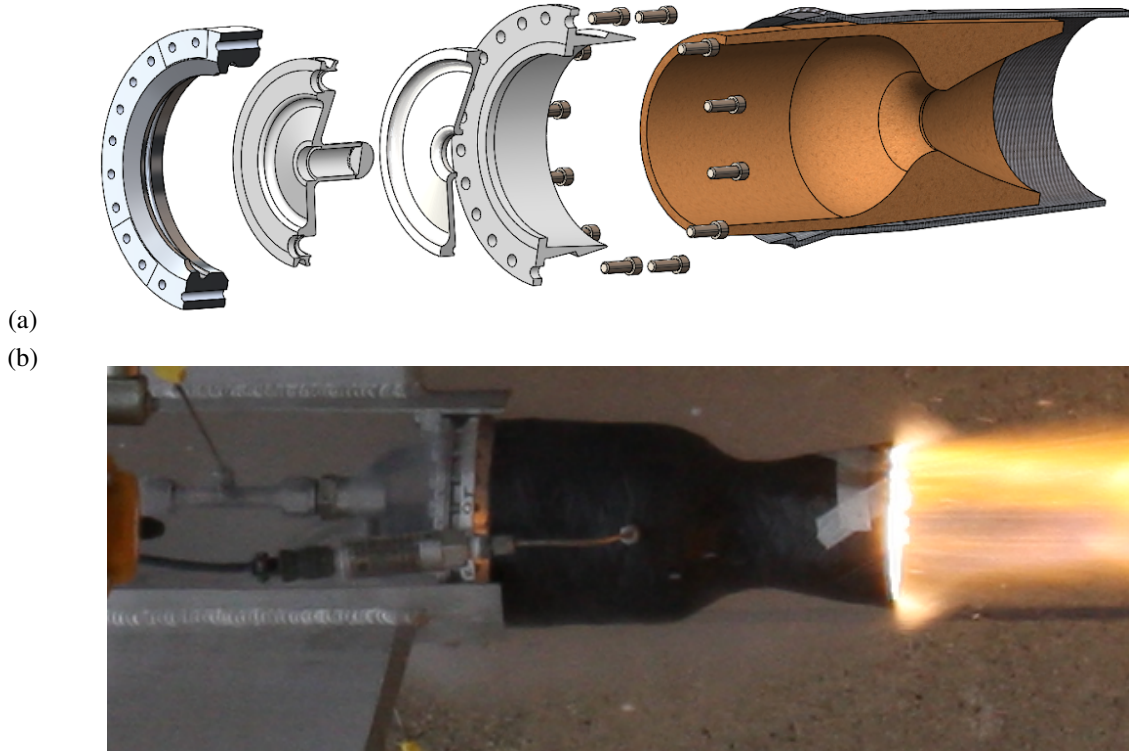


Fig. 4 (a) The flight weight engine assembly from Fall 2017 and (b) the final flight weight engine assembly from Spring 2018

The fire valves are modified Habonim C47 series ball valves with no cryogenic bonnet. These valves were special ordered to meet the needs of this rocket. While similar in appearance to other 47 series valves, the valves have the

internal packing of the cryogenic series of 47 series valves and custom fabricated end-caps that match the AS 1098B standard. These are pictured in Figure 5. To save weight and complexity of the flight vehicle, the actuator is fixed to the launch rail. The stem that interfaces between the actuator and the valve is slotted to allow the valve to slip past once the fire valves are opened and the rocket begins to travel up the rail.



Fig. 5 Flight valves installed on valve support ring

The use of coaxial propellant tanks is an exotic design choice that saves volume and fluid routing complexity, while offering potential benefits to fuel subcooling. Liquid methane at ambient pressure freezes at -296°F . Conveniently, saturated liquid oxygen at ambient conditions has a temperature of approximately -293°F . This allows for the methane tank to be inserted into the oxygen tank if sub-cooled oxygen is not being used, simplifying plumbing routes and providing opportunities to reduce weight due the stronger buckling strength of coaxial pressure vessels. The propellant tanks are made from Aluminum 6061-T6 using standard pipe stock and custom machined end caps. The liquid oxygen tank is 48" long and the liquid methane tank is 54" long. Both tanks have semi-domed caps and follow pipe code for the design tank pressures of 850 and 900 psi_a . The propellant tanks are pictured in Figure 6.



Fig. 6 (a) Top and (b) bottom of propellant tanks.

The tanks are pressurized using gaseous helium from a Luxfer composite tank with an internal volume of 285 cubic inches. The gaseous helium is stored at 4500 psi_a and sent through two Tescom BB-1 series regulators. Helium was selected over nitrogen as a pressurant due to the reduction in system mass and the decreased likelihood of condensation of the pressurant gas. The propellants are isolated from each other using Haskel cryogenic check valves. Mass flow rate of each propellant is controlled by a venturi installed at the bottom of each tank. Images of the upper and lower plumbing are presented in Figure 7.

Propellants are loaded via commercially available quick disconnects. These quick disconnects are mounted to linear pneumatic actuators that utilize 100 psia nitrogen. The pressurant velocity into the tanks is limited by diffusers attached to the boss fittings screwed into the top of the tank. An example of the quick disconnect and diffuser assemblies is



Fig. 7 (a) Upper and (b) lower rocket plumbing.

pictured in Figure 8.

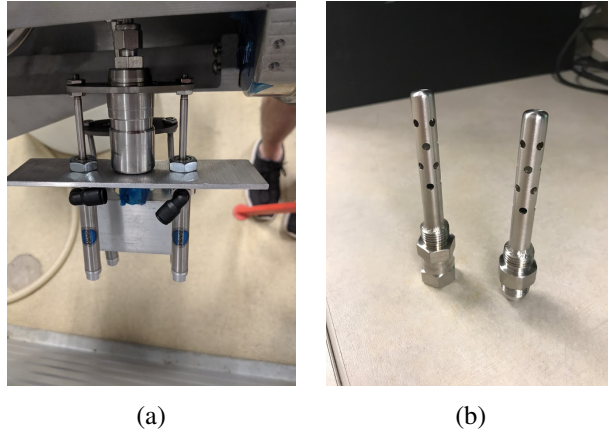


Fig. 8 (a) Quick disconnect assembly and (b) the diffuser assemblies

The quick disconnects have Teflon seats and Krytox 240AC lubricants, indicating compatibility with liquid oxygen. They are rated to actuate at pressures under 250 psia and are rated for pressures up to 1000 psia. The quick disconnect fitting and coupler are both self checking when disconnected. The helium quick disconnect is rated for pressures up to 6000 psia while connected but cannot be actuated unless it is vented. Additional plumbing on the ground support trailer supports venting the line prior to quick disconnect actuation. The helium quick disconnect is not self checking, necessitating a check valve downstream on the rocket.

B. Avionics System Overview

There are two distinct avionics systems installed on the vehicle. There is a recovery system mounted in the nose of the rocket and a flight computer for logging propulsion system data is installed just above the engine. These are pictured in Figure 9.

1. Flight Computer and Signal Conditioning

The flight computer is a Raspberry Pi 3B operating on the freely distributed Raspberrian operating system. A Measurements Computing Series 118 "Hardware on Top" (HAT) style analogue to digital converter (ADC) is installed on the Pi. This ADC supports recording data at 100k Samples/s and has eight analogue input channels for 0-10 VDC signals. The software employed on the Raspberry Pi is a modified python script, originally provided by Measurements Computing, that records the raw voltage from each channel in a comma separated list. The Raspberry Pi is capable of

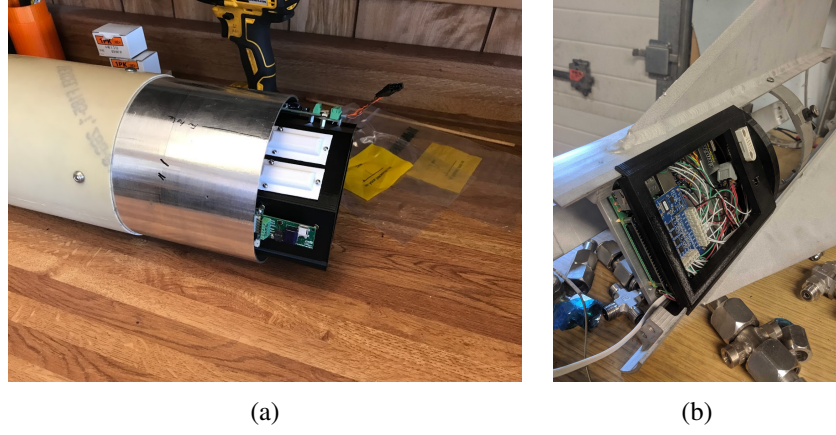


Fig. 9 The primary recovery avionics sled and the propulsion system data logger installed in their respective airframe sections.

writing data at a rate of approximately 2.5 kHz per channel. Data is recorded at 1 kHz per channel for the duration of the flight. The DAQ assembly is presented in Figure 10.



Fig. 10 The flight computer assembly

A magnetic umbilical is attached to the flight computer and allows data, power, and logic signals to be sent between the ground support and rocket DAQ computers. All data sent to the flight computer is sent in parallel to the ground support DAQ as a backup and to provide live monitoring from the data system operator's visual interface while the rocket is on the rail. Data logging is triggered by a 5 VDC logic signal sent from the launch trailer's computer during the launch autosequence, allowing the synchronization of data.

2. Instrumentation

The propulsion system is instrumented with one thermocouple and six pressure transducers. The thermocouple is a single 3" long Type-K Omega thermocouple inserted into the bottom of the oxygen tank. The methane tank does not allow for temperature instrumentation due to a design oversight. Therefore, the thermocouple in the oxygen is assumed to also be the temperature of the methane. This modification was made post stage testing to improve analysis of the flight system. The use of thermocouples on board required additional signal conditioning for the flight computer in the form of commercially available Adafruit 8495 boards.

The pressure transducers are GE UNIK 5000 series pressure transducers with built in signal amplification, outputting a signal on a 0-10VDC range. There are three pressure transducers at the top of the rocket and three at the bottom. The top three measure helium pressure and propellant pressures in the tank and are used to compute mass flow rate through the venturis. The bottom three measure propellant pressure entering the injector and chamber pressure. The injector manifold transducers are located just upstream of the run valves to allow for monitoring of the propellant fill activities



Fig. 11 Recovery system assembly

and to give an indication that propellants are being loaded. The chamber pressure transducer is a direct pressure tap but is on a 1/8" tube standoff that reaches into the airframe, a total length of approximately 10 inches.

The rocket instrumentation device types, scales, and accuracies [6] are presented in Table 1.

Table 1 Instrumentation Table

Instrument Type	Location	Range	Error*
TC	Oxygen Tank	-454 - 2300 °F	+/- 0.75%
PT	Helium Tank	0-5000 psia	+/- 0.2%
PT	Oxygen & Methane Tank	0-2000 psia	+/- 0.2%
PT	Injector Manifolds & Chamber Tap	0-1000 psia	+/- 0.2%

3. Recovery System Avionics

The recovery system features two, redundant altimeters for controlling deployment of the parachutes. They are powered by 2.7 VDC li-po batteries and feature remote arming from outside of the rocket. All recovery avionics are commercial off the shelf parts. More about the recovery system avionics is provided in the team's SciTech paper from earlier this year.[5]

C. Recovery System

In addition to the previously mentioned recovery avionics, the recovery system consists of a deployment mechanism and the parachutes themselves. The rocket is designed to utilize a dual deployment system, per competition requirements.[4] The complete recovery deployment system is pictured in Figure 11.

At apogee, the drogue chute and main chute are ejected from the recovery bay. The drogue unfurls but the main chute is held by a cord. Once the target altitude is reached, the recovery computer cuts the cord binding the main chute and the larger parachute deploys. This greatly reduces the drift of the rocket while maintaining a low enough velocity to deploy the larger parachute without shearing the bolts or snapping the tethering cable. For launch this year, a single parachute may be utilized since the expected altitude is significantly reduced from the target altitude of 45,000 feet. Justification for this is discussed further in the Static Fire Testing and Flight Profile sections of this paper. Additional details about the recovery system is provided in the team's SciTech paper from earlier this year.[5]

D. Airframe

The airframe was designed to allow for modular assembly of each rocket system. It is sectioned and denoted as the lower, middle, and upper airframes. The lower airframe is the fin can, the middle airframe is just forward of the propellant tanks, and upper airframe is forward of the recovery deployment bulkhead. With the exception of the nose

*Full scale accuracy error

cone, all airframe parts are made from either Aluminum 6061-T6 or 7075-T6. Each major airframe section's location is provided in Figure 12.



Fig. 12 Major components of the rocket airframe and their location

The lower airframe is the fin can and consists of three thrust bearing columns with fins welded to the exterior, three 1/16" thick panels, and a structural support ring that also serves to fix the rocket to the launch rail and hold the run valves in place. This structure transfers the load of the engine to the propellant tanks via tabs on the inside of the fin columns. These tabs are secured to the tank and the engine with axial bolts. The middle airframe provides support structure for the pressurant tank and plumbing. It is approximately 42 inches long and has three access panels for manipulating plumbing and instrumentation. This structure fits over the top of the tank and is secured with radial bolts. A clocking feature locks its rotation in place for consistent assembly. The upper airframe is a simple cylinder within cylinder assembly that attaches to the mid airframe via a coupler and radial bolts. The nosecone and ejection bay slide into the parachute bay and are held in place by the aerodynamic forces on the rocket.

These modular sections allow for each subsystem contained within to be assembled, checked, and prepared prior to final rocket assembly. The airframe is discussed further in sections A through D of the team's 2019 SciTech paper.[5]

E. Ground Support System Overview

The ground support system provides the capability of remote propellant loading and launch of the sounding rocket. There are two subsystems to the ground support equipment: the propellant handling and the data acquisition and control system.

1. Propellant Loading and Conditioning System

The ground support system is capable of loading liquid oxygen, liquid methane, and gaseous helium into the vehicle. Liquid oxygen and gaseous helium are both commercially and readily available in Indiana. These fluids are purchased in dewars and K-Bottles and delivered to the launch site. They are tied into the trailer which has remotely operated valves for the loading of propellants. The P&ID's for these fluid systems as installed on the GSE trailer are presented in the Appendix in Figures 26 and 27.

Liquid methane is challenging to purchase in a pure form. Previous work at Purdue University had developed the capability to condense gaseous methane into liquid form for use in a variety of projects, most notably in the development of the Morpheus thrust chamber.[1] Based on this development work, a scaled up system was designed for use on this project and future projects. A methane condenser was designed to operate at working pressures of up to 5000 psi_a , support flow rates of up to $6 \frac{\text{lb}_m}{\text{s}}$, and store up to 9 lb_m of liquid methane in a reserve tank. These numbers were in anticipation of the future development of a larger engine by students but also conveniently supports rapid fueling of the sounding rocket presented within this paper. A P&ID for this system is presented in the Appendix in Figure 28.

The liquid methane condenser consists of two fluid systems in a boil-off style heat exchanger. Gaseous methane is fed into the condenser which is submerged in a liquid nitrogen bath. The pressure on the bath is controlled by a precision, computer controlled needle valve. By balancing the pressure of the liquid nitrogen, methane can be conditioned to a desired temperature and effectively sub-cooled. The nitrogen jacket is maintained at a pressure greater than 60 psi_a in order to avoid freezing the methane; the saturation temperature of liquid nitrogen at this pressure corresponds to the freezing point of ambient methane.[7] [8] Due to the usage of methane filters submerged in the liquid nitrogen, frozen methane will result in a blockage and reduced flow capacity throughout the system.

2. Data Acquisition and Control

The data acquisition and control (DAQ) system employed on the launch system is heritage design of Purdue University's Maurice J. Zucrow Laboratories, an iteration based on the DAQ built for use in experiments by Dr. Brandon

Kan. The system takes advantage of National Instruments USB DAQ hardware for ease of use and modular, smaller design. All digital and analog inputs and outputs are sent to terminal blocks enabling quick manifolding of each channel's power and signal. Thermocouple signal conditioning is accomplished using a GE FANUC signal conditioning unit with built in reference junction, housed in a secondary junction box. The ground support system supports 32 analogue inputs, 8 analogue outputs, and 32 digital outputs. Analogue inputs provide temperature, pressure, and other instrumentation readings. Analogue outputs are used for electronic regulators and control valves. Digital outputs are used for two state pneumatic valve actuation. Data is acquired at a sample rate of 1 kHz per channel. Images of these two systems are presented in Figure 13.

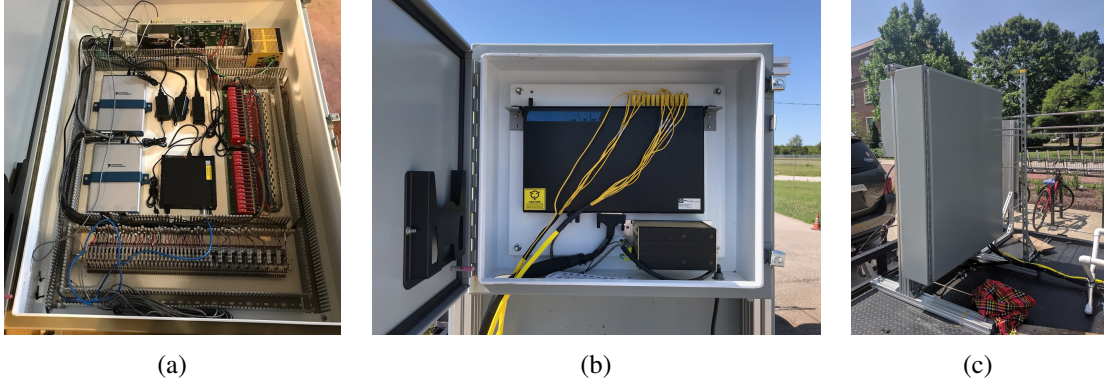


Fig. 13 From left to right: DAQ, Thermocouple Signal Conditioning, and Installation on Trailer

The critical design feature is the ability to shut off power to all valves and revert them to their default, de-energized state while also maintaining instrumentation readouts. This is accomplished by the simple use of dual 24 VDC power circuits, one for valves and one for instrumentation. A kill switch tied in series with the valve power supply ensures that in the case of an emergency all valves can be quickly killed at the flick of a switch.

The software employed for data acquisition is an in-house code developed in LabVIEW by Mr. Brent Justice and other students at the lab. The code allows for the use of multiple NI devices and cards at multiple acquisition rates, in addition to allowing for auto-sequenced testing and various triggered events based on instrumentation readouts. A brief overview of the capabilities of the Zucrow data system architecture is given in [9].

V. Modeling and Simulation

A. Vehicle Dynamics

The vehicle was dynamically modeled using a simple, 2-D altitude model developed in MATLAB and verified with OpenRocket, an all-purpose design tool used in the aid of amateur solid-rocket design developed by students at Helsinki University of Technology.[10] A free body diagram of the rocket motion is presented in Figure 14.

The equation of motion is compiled below from this free body diagram and presented in Equation 1:

$$du = \frac{-u_e dm_v}{m_v} - \frac{D}{m_v} dt - g \cos \theta dt \quad (1)$$

Where u is the change in vehicle velocity, u_e is the exhaust velocity, m_v is the vehicle mass, D is the drag force, t is time, g is gravitational acceleration constant, and θ is the difference between the rocket's direction of travel and a vertical flight path. The equation of motion is evaluated using MATLAB's ODE45 solver for numerical analysis of the system due to the inclusion of drag. Drag coefficients were estimated for various altitudes based on relations obtained from Fleeman [11] and then later verified with OpenRocket evaluations. For all simulation runs used to evaluate rocket altitude, the angle relative to the ground was set to zero, that is $\theta = 0$.

A basic optimization was run to evaluate the major parameters of rocket sizing: O/F, mass flow rate, chamber pressure, expansion ratio, and tank operating pressure. Thrust was fixed for all parameter sweeps. An executive decision was made early in the program to fix the thrust level of 1125 lb_f , or 5 kN. The injector ΔP was fixed similarly to thrust at 20%. Estimates of pressure drops were constructed from notional line lengths and the diameter was established to



Fig. 14 Free body diagram for the rocket system

keep the liquid line velocity below $20 \frac{ft}{s}$, a guideline imposed upon all designs at Zucrow. The venturis were assumed to have a 15% ΔP across them in order to allow for continued cavitation.

A sizing code was constructed around the parameters previously mentioned and was used to estimate the rest of the vehicle mass. It utilized NASA CEA code and applied estimated efficiency values taken and inferred from Sutton and Biblarz.[12]

B. Engine Sizing

The engine sizing requires the input of several set design parameters and assumptions. These include estimates of C^* and C_f efficiencies, a value of L^* , a value for mixture ratio, a value of chamber pressure, a value of thrust, and a target expansion pressure. These design variables can be manually supplied or provided from the optimization code.

With these values and with propellant properties entering the engine, a call to the NASA CEA code is made. The outputs from this code include the value of expansion ratio, C_f , C^* , and I_{sp} . The assumed efficiencies are applied to the last three parameters, such that an estimate for the "real" value can be applied to the system. The equations for these are given below:

$$C_{f,real} = \eta_{C_f} C_{f,CEA} \quad (2)$$

$$C_{real}^* = \eta_{C^*} C_{CEA}^* \quad (3)$$

$$I_{sp,real} = \eta_{C_f} \eta_{C^*} I_{sp,CEA} \quad (4)$$

With these parameters determined, the engine can be sized. The first and perhaps most important value is the size of the throat.

$$A_t = \frac{F}{P_c C_{f,real}} \quad (5)$$

With the result of Equation 5, and by assuming a contraction ratio, the chamber length and the chamber diameter can be determined using Equations 6 and 7.

$$L_c = L^* / C_r \quad (6)$$

$$d_c = \sqrt{A_t * C_r * 4/\pi} \quad (7)$$

The required mass flow rate for the system is determined using Equation 8,9, and 10. Note that the use of the "real" value for I_{sp} results in accounting for potential performance losses.

$$\dot{m}_{tot} = \frac{F}{g_0 I_{sp,real}} \quad (8)$$

$$\dot{m}_f = \dot{m}_{tot} [1 + (O/F)]^{-1} \quad (9)$$

$$\dot{m}_{ox} = \dot{m}_f (O/F) \quad (10)$$

Lastly, the required feed pressure into the injector is computed simply using Equation 11.

$$P_{inj} = \frac{P_c}{1 - \frac{c_{\Delta P}}{100}} \quad (11)$$

Where $c_{\Delta P}$ represents the design pressure drop percentage. With these values computed, the fluid system components can be sized.

C. Fluid Components Sizing

Moving upstream from the engine, the next components to be sized are the run lines. Per a design philosophy of Zucrow Labs, the flow speed was initially sized to be less than 20 ft/s. Flow speed, v , was computed from continuity:

$$\dot{m} = \rho u A \quad (12)$$

The resulting pressure drop in the line was estimated on a per length basis in order to estimate the total pressure budget needed. It was computed with Equation 13, shown below.

$$\frac{\Delta P}{L} = \frac{-2\rho u^2 f_d}{D_H} + \rho \left(\frac{F}{m} - g_0 \right) \quad (13)$$

Where L is the length of the tube section, f_d is the Darcy friction factor, D_H is the hydraulic diameter, F is thrust, m is the rocket mass, and g_0 is the acceleration due to gravity. The second term only applies if the tube is oriented in the direction of rocket travel. To compute these values, NIST's REFPROP was called to get fluid properties required to compute intermediate values, including Reynolds number and f_d .

Tube wall thicknesses were obtained using MS-01-107 charts for seem-less stainless steel tubing converted into a tubing guide.[13] The line velocity requirement establishes the tube minimum inner diameter and the pressure budgeting determines the required wall thickness. Tubes are compared and selected provided they meet both requirements. For sizing code, bend radius requirements and minimum lengths for flaring and wrench clearances were not considered. These are equally as important for final design and many of the sizing code outputs were used more as guidelines in order to meet these additional requirements.

1. Valve Sizing

Valves were sized to obtain the required flow coefficient, C_v , in order to maintain a ΔP less than 1% of the tank set pressure. The equation for C_v is presented in Equation 14:

$$\Delta P = G \left(\frac{\dot{Q}}{C_v} \right)^2 \quad (14)$$

Where G is the specific gravity of the fluid, \dot{Q} is the volumetric flow rate in GPM, and C_v is the desired flow coefficient of the valve.

2. Venturi Sizing

Mass flow rate was controlled using venturis. These were sized per cavitating venturi flow rate governing equation, found in [14] and [15], presented in Equation 15.

$$\dot{m} = C_d A_t \sqrt{2\rho(P_1 - P_v)} \quad (15)$$

Where C_d is the discharge coefficient, A_t is the venturi throat diameter, P_1 is the upstream pressure, and P_v is the vapor pressure of the fluid. The discharge coefficient from the venturi is given from the vendor but can be verified using water flow testing with a catch and weigh setup. The other properties are pulled from REFPROP. This same equation is later used to compute mass flow rate in the system using measurements from instrumentation. The pressure drop across a venturi is assumed to be 20% or greater when cavitating.[16]

3. Tank Sizing

The fluid component sizing provides the total pressure budget required for the rocket, setting the propellant tank's desired pressure. The propellant tanks were designed to be approximately equal in length to make fabrication of the coaxial tanks easier. The volume required for each tank was taken from the mass of loaded propellant, divided by density, and the multiplied by a factor of the required ullage space.

$$V_{tank} = c_{ull} \frac{m_{prop}}{\rho_{prop}} \quad (16)$$

Since the outer tank was both structural and coaxial, it has the outer diameter of the rocket and the inner diameter equal to outer diameter of the second propellant tank. From basic geometry for cylinders, the tank length is:

$$L_{tank} = \frac{V_{tank}}{\frac{\pi}{4}[(d_o - 2t_w)^2 - d_i^2]} \quad (17)$$

Where d_o is the outer diameter, t_w is the wall thickness, and d_i is the inner diameter. For the inner tank, d_i is set to zero. The required pressurant was sized from balancing the following equation:

$$P_1 V_1 = P_2(V_1 + V_2) \quad (18)$$

Where P_1 is the initial helium tank pressure, V_1 is the volume of the helium tank, P_2 is the desired tank pressure, and V_2 is the volume of the propellant tank. This method does not account for cooling of the pressurant as it comes in contact with the cryogenic propellant, something that must be accounted for as shown in the results of the first stage hotfire.

All tanks were initially analyzed using thin wall pressure vessel analysis for cylindrical pressure vessels. This was analyzed using the following equation for hoop stress found in [17].

$$\sigma_\theta = c_{safety} \frac{P(d_o - t_w)}{2t_w} \quad (19)$$

Where P is internal pressure and c_{safety} is the safety factor. These were initially analyzed using a safety factor of two and comparing it to the allowable stress in the material. Later, the tanks were redesigned using the ASME B31.3 pipe code, significantly increasing wall thickness. However, this design change occurred post-PDR and was not accounted for in the initial sizing code used to predict altitude.

D. Structures

Vehicle structures were initially estimated as cylindrical columns in a simple buckling analysis. The buckling equation was referenced from [18] and is presented in Equation 20.

$$F = \frac{n\pi^2 EI}{L^2} \quad (20)$$

F is the allowable load, n is an end condition factor, E is the modulus of elasticity of the material, I is the moment of inertia of the column, and L is the length of the column. The moment of inertia set the geometry of each structural part. Later, the final designs were analyzed using a combination of ANSYS and SolidWorks structural analysis tools given their more complex shape. A buckling safety factor of two or greater is maintained on all structures.

E. Mass Estimates

With most major components sized, their masses were computed from previously defined geometry and material density. This estimation included tubing, tanks, and major airframe components. Complex geometry was estimated using SolidWorks mass estimators for parts and added to the vehicle mass manually. Fitting, valve, and regulator masses were estimated from similar components on hand or component catalogs. The recovery system masses were also taken from components already on hand or from information available from the vendor. The payload was specified in the competition requirements [4]. The initial propellant mass was estimated using the volume of the tank (non-ullage) and the desired temperature for propellants in their pre-pressurization state. The mass of the helium in the system was taken from ideal gas law. For simulations, mass was updated assuming a constant mass flow rate of oxygen and methane. Pressurant mass does not change in the system until after burn out and was held constant throughout the simulation.

F. Sizing Code Results and Limitations

The rocket sizing and analysis code quickly iterated through the suite of design variables and produced an output that would serve as a guideline for all final design decisions. The following are the iterated design variables, the sizing code result, and the final design value from the system's critical design review.

Table 2 Sizing code outputs

Parameter	Code Result	Final Value
O/F	2.97	2.9
P_c	550 psia	550 psia
ϵ	6.7	6.7
d_o	6"	6.42"
L_{rocket}	15'	15'
\dot{m}	4 lb _m /s	4.12 lb _m /s

The code also predicted that 125 lb_m is the largest GLOW that can successfully meet the minimum target altitude of 30,000 feet if the performance matches the predictions. Given that the rocket is nearing final assembly, but is not quite complete, a final value of mass is not yet known. Currently, the final rocket GLOW is estimated to be 120 pounds.

The major limitation of this sizing code is the difficulty translating the required design values to physical hardware. The sizing code is an ideal, optimistic look at the rocket system. Many things were unknown as the code was written, including the likely-hood of meeting the predicted performance values. Thus, the sizing code was treated more as a guideline rather than a hard and fast design value. As shown later in the testing section, actual performance of the propulsion system is significantly lower than required to meet competition requirements for altitude. For future designs, a heavy amount of pessimism is recommended.

VI. Manufacturing and Prototyping

The fabrication of the Purdue Liquid Methane, Liquid Oxygen Sounding Rocket presented unique challenges. Fabrication was largely accomplished utilizing university resources, including student and professional machine shops. The majority of fabrication was accomplished by students at the Bechtel Innovation and Design Center (BIDC), professional machinist Jerry Hahn at the Aerospace Sciences Lab (ASL), and professional machinist and welder Rob McGuire at Maurice J. Zucrow Labs. Manufacturing for the rocket began in January 2018 and concluded with the first full-stack test in May 2018. During that period 38 unique parts were manufactured by students or professional machinists. Collectively, students volunteered over 700 hours in the BIDC and other locations on campus to contribute to the completion of the rocket. Based on standard manufacturing labor costs, this reduced the cost of the project by an estimated \$54,000.

A. Engine

The flight engine consisted of two assemblies. The injector assembly was manufactured at Purdue University's Aerospace Sciences Lab by Mr. Jerry Hahn. It consists of two stainless steel 17-4 PH wetted enclosures for propellants and an unwetted structural ring fabricated from Aluminum 7075. A manifold for the oxidizer was constructed out of

stainless steel tubing, a stainless steel billet, and a modified JIC 514 fitting welded together to support distribution of the liquid oxygen to two points on the injector. The fuel has a single JIC 514 fitting welded in place at the top of the pintle. The welding was completed at Maurice J. Zucrow labs by Mr. Rob McGuire.

The chamber consists of an Aluminum 7075 flange and a composite over-wrapped ablative liner mated to the flange. The flange was fabricated in house at BIDC by students on the team. The chamber was constructed by Mr. Dan Moser of Compositex. A total of two chambers were fabricated. The first one was consumed in stage testing of the vehicle. The second was fabricated for flight. SN02 features some modifications to materials of construction to improve regression rate.

B. Tanks

The rockets concentric integral tanks presented a challenge that was overcome through the combined effort of student and professional manufacturing. The tanks were comprised of 6 Aluminum 6061-T6 components. Two end caps on the top and bottom of the tank, two for LOX and two for methane, and aluminum pipes that comprised the body of the tanks for each fuel. The end caps required tight tolerances for complex geometry but students were able to develop a process that utilized both CNC Mills and Lathes at the BIDC to produce these parts within requirements. However, student volunteers did not have the experience in welding required to join these parts to their tanks. The professional welding work was donated by North Mechanical Contracting of Indianapolis.

C. Recovery

The design of the recovery system required only one part, the recovery bulkhead, to be manufactured by students at the BIDC. This part interfaced with commercial products that operated the deployment of the recovery system. Light assembly was required to produce a fully capable system.

D. Avionics

The data collection electronics were secured within the rocket by a light sled that attached to parallel bolts through the recovery and payload bulkheads. This sled was 3-D printed on a students personal 3-D printer using PETG filament. Avionics were secured with zip ties or glued in place.

A second sled for propulsion data measurement was installed just above the engine. A base-plate, made of Aluminum 6061-T6, was fabricated to allow all components to be mounted to it prior to installation in a plastic case. The case was also 3-D printed using PETG filament. The electrical components were installed on the exterior facing side of the plate and Amphenol through-wall connectors were installed on the interior facing side. These connectors were used to interface with the system's six pressure transducers installed for flight measurement. An additional two pass throughs for Type-K thermocouples were installed in a pocket milled out to fit standard omega through wall clips. The flight computer and data acquisition HAT were installed using steel standoffs. Additional standoffs were used to mount the thermocouple signal condition blocks. A second plastic piece clips into the case and friction fits the case to the airframe.

E. Structures

Structures required the largest amount of total manufacturing and likewise utilized the resources available at the BIDC more than any other subcategory of the rocket. The fins, fin bases, mid-airframe, upper-airframe, and several critical bulkheads were manufactured by students at the BIDC. Requirements for all parts were easily satisfied by the capabilities at the BIDC with the exception of the mid-airframe, which required 4-axis CNC support. Existing machines at the BIDC did not have both the 4-axis capability and the work volume required to manufacture the component. This challenge was overcome by installing a 4-axis rotary in a larger 3-axis mill that fit the length of the mid-airframe.

F. Ground Support Equipment Trailer

The ground support system has several sub-assemblies that were fabricated over the period of a year and a half. The major components consist of the DAQ, the condenser, the valve paneling, and the feed plumbing. These are, in turn, installed on a 17' flat bed trailer. The DAQ was completed by students at the lab. The condenser, presented in Figure 15, was completed through the combined effort of students, Mr. Rob McGuire's machining skills, and the welding capabilities of North Mechanical Contractors.

The valve paneling was completed by students and installed on the trailer in Spring 2019 and is presented in Figure

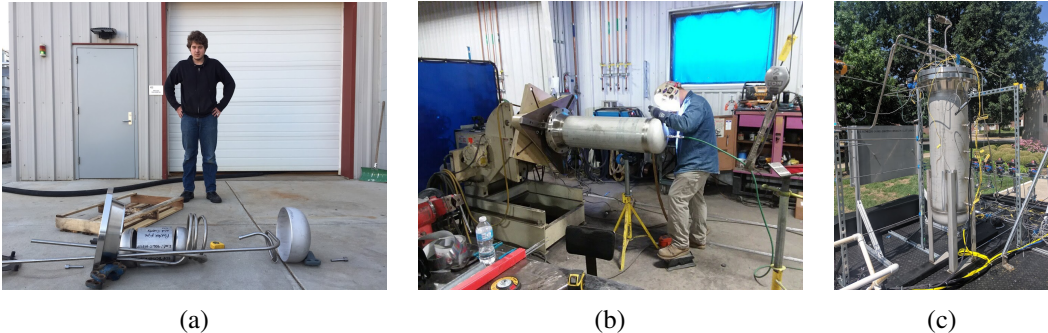


Fig. 15 From left to right: Condenser components, condenser fabrication, and condenser assembly installed

16. These panels were fabricated from parts salvaged from previous experiments at Purdue University. Components using oxygen were rebuilt and cleaned. The valves are installed on Aluminum 6061-T6 panels and supported by 80/20 extrusions bolted to the trailer floor.

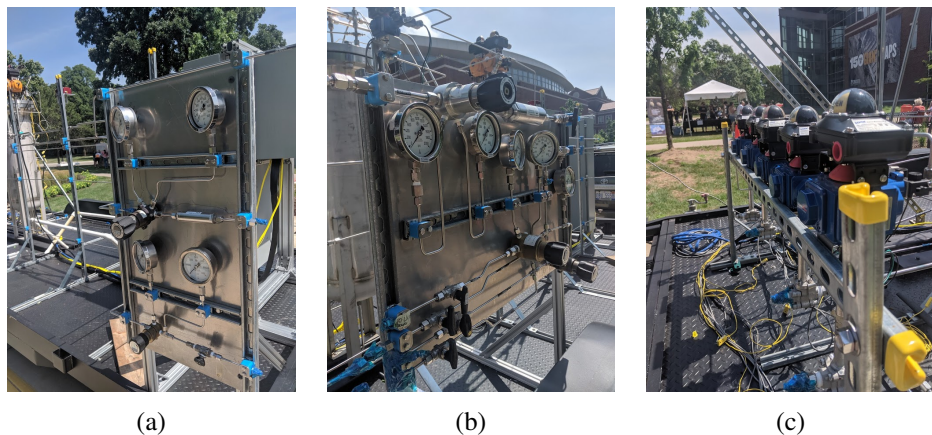


Fig. 16 From left to right: Helium and pilot loading panel, main methane and purge control panel, remote actuated valve fixture for fill and vent control

The feed plumbing was installed onto the trailer by students in Summer 2019. All lines utilized stainless steel tubing to accommodate the four different fluids used in the vehicle. The tubes are rated up to 3700 psi_a minimum as per the Swagelok allowable working pressure catalog, with the helium line rated up to 5100 psi_a . Students secured the lines by installing unistrut assemblies across the trailer to hold tube clamps. Army-Navy (AN) joint fittings were primarily used in the plumbing assembly due to ease of assembly, low cost, and access to automatic flaring machines at Zucrow Labs. In cases such as the high pressure helium and gaseous methane lines, o-ring face seal fittings were utilized to minimize leaking.

Students cleaned the lines and fittings on the trailer to remove FOD and prevent unwanted and unanticipated ignition in the oxygen lines. The fuel and inert gas lines were cleaned by pushing a clean-room wipe soaked in isopropyl alcohol down the length of the tube using compressed air, repeated three times. The helium, nitrogen, and liquid oxygen lines were cleaned by either a sonic bath in Navy Oxygen Line Cleaner or flowing an all-purpose cleaner through the longer components. Both processes were finished by rinsing the component in de-ionized water and drying with gaseous nitrogen. Once clean, the lines were only handled while wearing nitrile gloves and ends were sealed with flash breaker tape which leaves minimal residue on the surface of the tube.

VII. Component and System Level Testing and Analysis

A. Boilerplate Engine

A boilerplate engine was tested in February of 2018 at Maurice J. Zucrow Labs on the "10K" stand. The objectives of the test were to gain team experience in conducting high pressure, dual cryogenic tests and to qualify the injector design before proceeding with fabrication of a flight weight injector. The engine was made of schedule 60 medium grade carbon steel pipe welded to a standard concentric reducer with roughly the same dimensions as the flight-engine design. The entire chamber had the same L* as the final engine design. Due to the objective of this test, the chamber was without any expansion. The chamber ended at the throat, with a welded flange allowing for pressure tests. The chamber was fitted with a standard 1/8" pressure port. The engine was successfully fired for 0.4 seconds at lower O/F than nominal flight conditions. The results of these tests are compiled with the static fire testing results later in this section. Significant melting was observed in the throat of the chamber.

B. Boilerplate Injector Damage Characterization

A unique opportunity afforded by Purdue's facilities was ultra-high-resolution electron microscopic analysis of the injector pre- and post-hotfire. Due to the extreme environment seen by the injector, this was the lowest confidence part, and detailed analysis of the injector was desirable, especially considering that the test hot-fire had significantly melted a portion of the throat of the carbon steel chamber.

The goal of this analysis was to identify any micro-structural fractures, stresses, or corrosive failure mechanisms that may have occurred during the hotfire.

This project utilized two microscopes. A FEI Teneo FEG Volumscope was used for Tomographic imaging via Secondary Electron Detection. A FEI Quanta FEG Dual Beam was used for elemental analysis via Back-Scatter Electron Detection and Energy Dispersive X-Ray Analysis.

1. Topographical Pintle Analysis

In order to establish a baseline comparison, a hole pattern identical to the pintle's hole pattern was machined into an SS 316 sample piece. As seen in Figure 30, there are a number of topographical artifacts left over by the manufacturing process, including surface scoring and edge wear, that are important to identify as to not misidentify damage on the post-fire injector.

After the test fire of the boilerplate, the engine was disassembled, and the injector placed in the Teneo Volumscope for initial analysis, as seen in Figure 17. A full 360° scan of the pintle tip was performed. Despite superficial discoloration in the tip, practically no structural damage was observed, in particular no micro-structural fractures or melting.

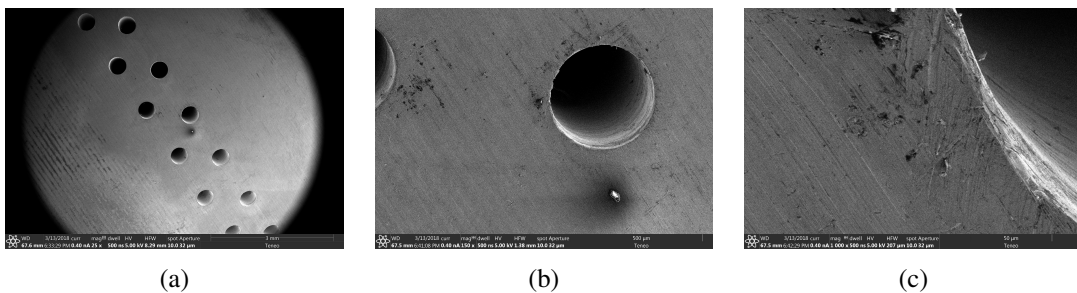


Fig. 17 Images captured by the Teneo Volumscope of the post-fire pintle at: (a) 50x magnification (b) 150x magnification and (c) 1000x magnification.

There was pitting corrosion observed around the pintle holes, likely due to the oxygen-rich atmosphere of the pintle, and imperfections in the steel used. However, this damage was insignificant enough to not present an issue, even with respect to the multiple injector hot fires that the flight weight design would undergo.

2. Topographical and Elemental Injector Face Analysis

The injector face was also a crucial part of the injector, and therefore was also imaged for structural damage or other failure mechanisms. When the boilerplate engine was disassembled, a certain buildup was noticed on the

combustion-side face of the injector. This was most likely the throat of the engine, which had melted during the test fire, but analysis was required to provide evidence for this theory.

In Figure 18a, the oxygen-facing side of the injector can be seen at 3000x magnification. Here, the manufacturing marks can be observed, but little else can be seen with regards to failure mechanisms or debris. Figure 18b is the combustion-facing side of the injector, and here the buildup can be observed. However, a thorough analysis of the face of the injector revealed no failure mechanisms, nor even the poring effect that was observed on the pintle tip. Therefore, from a structural standpoint, the injector was deemed a success.

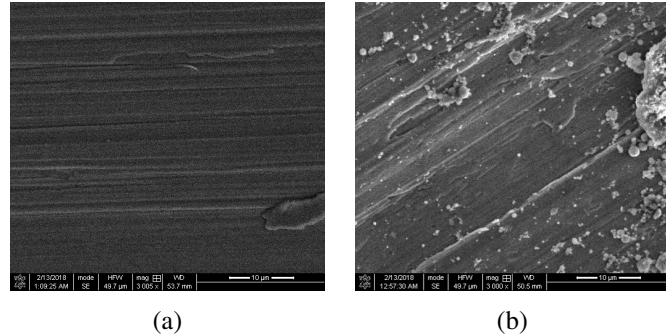


Fig. 18 Comparison of (a) the oxygen-facing side of the injector face, and (b) the combustion-facing side of the injector face. The oxygen face was imaged to provide a baseline comparison for any damage incurred to the face during the hot fire. Both images are taken at 3000x magnification

In order to identify the buildup on the injector face, a sample of about 1mm diameter was taken, and placed in the Quanta FEG microscope for EDX analysis. These sample images can be seen in the Appendix in Figure 31a, and one of the areas of the sample chosen for elemental spectrum collection can be seen in the Appendix in Figure 31b.

The EDX spectrum collected from the site can be seen in the Appendix in Figure 32. The four statistically significant elements are Iron (65.45%), Oxygen (25.45%), Carbon (16.49%), and Silicon (3.1%). The silicon is an artifact present in many post fire engine components, and exists as a result of o-ring rubbing in the valves and flanges of the fluid system.

Additionally, the only other element observed that can't be discounted due to signal noise is magnesium, which is a standard component of Carbon Steel, the material used for the boilerplate engine, supporting the idea that the buildup on the face of the injector was the result of the melted throat recirculating and depositing on the injector face. Further evidence of this theory can be seen in the Appendix in Figure 33, which displays the concentration of the individual component concentrations. Iron, the dominant component of Carbon Steel, is omnipresent throughout the sample, while Carbon, present in large quantities in both the Carbon Steel and the Methane fuel, is concentrated only the bottom of the sample- the side that was touching the SS316 injector face, which suggests that it was not deposited there by the combustion process. Oxygen, however, is present in concentration only on the top and sides of the sample, which suggests that the sample was immersed in an oxygen rich environment. This area is most probably the oxygen-rich re-circulation zones typically associated with pintle injectors.[19] This idea is supported by the fact that the silicon follows a nearly identical deposition pattern to the oxygen, as the silicon, which would have been transferred into the chamber by the fuel and oxidizers, was present only in the combustion gasses, and not in the chamber walls, and acts as an elemental marker for the presence of combustion gasses.

Therefore, it was concluded that the injector buildup was an artifact of the melting of the throat of the boilerplate engine, and would not present an issue in the final engine. Since pitting corrosion was the only failure mechanism observed, and only present around the pintle's injection holes, it was ultimately decided that the pintle injector met the design criteria for further testing in the flight weight engine.

C. Recovery Ground Tests

A series of recovery ground tests were conducted to verify the parachute deployment mechanism worked in each of its respective steps. The CO₂ canister mechanism, the CO₂ ejection assembly, the deployment charges, and the main parachute unfurling were all tested separately. These tests are shown in Figure 19.

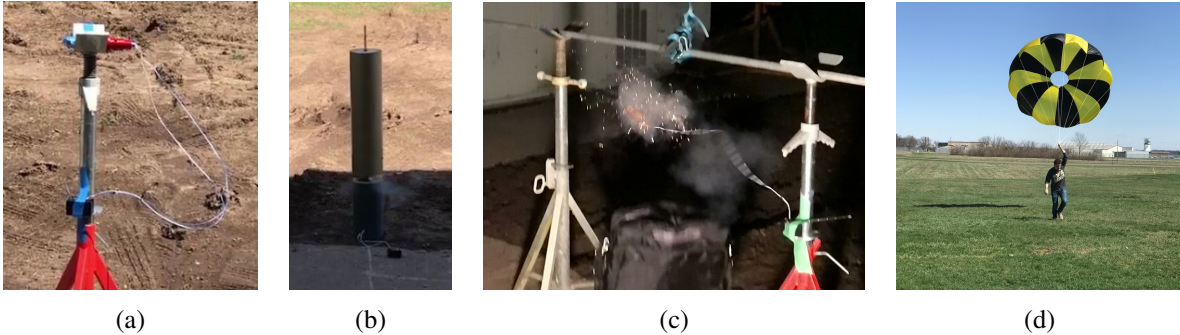


Fig. 19 (a) CO₂ cannister actuation test and (b) CO₂ ejection test, (c) deployment charge testing, and (d) main parachute deployment testing

D. Tanks

The propellant tanks were each hydro-proofed to a safety factor of 1.5 of expected operating pressure using a high pressure water pump. The test apparatus consisted of a fill valve, a relief valve, and a bleed in valve. The tanks were shaken during fill to remove as much air from the system as possible to reduce the chance of pneumatic decompression should a leak or failure point be found.

While the proofing of the Luxfer composite tank went off smoothly and without any events, the proofing of the coaxial tanks proved to be a challenge. The tanks were designed to be proofed individually to the desired pressure. The inner tank was proofed first and passed without event. The outer tank, upon pressurization to 500 psi, refused to increase in pressure indicating that there was leak. Upon initial inspection, no source of liquid displacement could be found. A second attempt was made but the pressure only increased to 300 psi. Upon closer inspection, it was found that the inner tank was collapsing due to the external pressure. The inner tank was then re-hydro-proofed per procedures. Fortunately, it again met the required pressure and held for five minutes without incident. Both tanks were then filled with liquid water and pressurized. The propellant tank hydroproofing setup is shown in Figure 20.

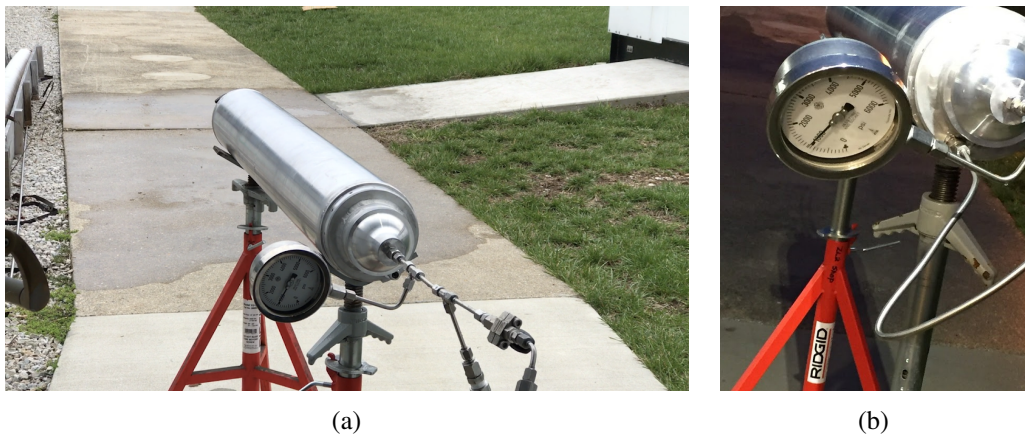


Fig. 20 (a) Hydroproofing setup for center tank and (b) hydroproofing test setup for both tanks

This was an important lesson for the team. While it was understood that the design was optimum for a lower pressure difference across tanks, the implications of external pressure on the depressurized inner tank weren't fully realized until the tanks were nearly destroyed. Future procedures for coaxial tanks call for the proofing of the inner tank and then both tanks to verify that the two are isolated from each other and can hold pressure.

E. Static Fire

Two static fire tests were conducted on the propulsive system in mid-2018. These tests were to measure the total impulse of the system and verify the performance of the integrated propulsion system. Both tests were functional tests

of the ground support equipment, data acquisition system, rocket propulsion system, and avionics system. Images from the second of these tests are included in the Appendix in Figures 34 through 39.

The real system efficiency values were computed using Equations 2, 3, and 4. The recorded value of chamber pressure and thrust, calculated values of mass flow rate, and the measured value for throat and exit area were all inputted into NASA's CEA code. In order to get the real value for C_f , C^* , and I_{sp} the following equations were employed, taken from Appendix 3 of Sutton and Biblarz.[12]

$$C_{f,real} = \frac{F}{P_c A_t} \quad (21)$$

$$C_{real}^* = \frac{P_c A_t}{\dot{m}} \quad (22)$$

$$I_{sp,real} = \frac{F}{g_0 \dot{m}} \quad (23)$$

The following tables, Tables 3 & 4, present the time-averaged values of engine and propulsion system performance. Plots of these values with respect to time are presented in the team's SciTech paper from earlier this year.[5]

Table 3 Time averaged performance values from Spring 2018 testing

Test	Engine	t_b	$D_{t,0}$	P_c	O/F	C^*	I_{sp}	Thrust	η_{C^*}	η_{C_f}	$\eta_{I_{sp}}$
Design	Flight	8.1 s	1.32 in	550 psi	2.9	5400 ft/s	275 s	1125 lb _f	0.90	0.95	0.86
1	Dev	0.4 s	1.34 in	430 psi	2.5	5367 ft/s	106 s	384 lb _f	0.885	0.950 [†]	0.841
2	SN01	5.1 s	1.32 in	237 psi	3.0	4166 ft/s	180 s	536 lb _f	0.689	0.915	0.630
3	SN01	8.2 s	1.68 in	171 psi	2.5	5026 ft/s	187 s	532 lb _f	0.832	0.846	0.705

Table 4 Regression rate analysis from Spring 2018 testing with chamber SN01

Test	t_b	$D_{t=0}$	$D_{t=t_b}$	$\varepsilon_{t=0}$	$\varepsilon_{t=t_b}$	$\frac{\Delta r_t}{\Delta t}$
Design	8.1	1.320 in	1.368 in	6.7	6.2	0.003 in/s
2	5.1	1.320 in	1.628 in	6.7	4.6	0.030 in/s
3	8.2	1.628 in	2.060 in	4.6	2.9	0.026 in/s

Table 3 paints a bleak picture of the flight propulsion system's performance. The thrust and chamber pressure were significantly lower than the design point for the duration of both system level hot fire tests. This poor performance has two root causes: pressurant collapse in the cryogenic tanks and greatly increased regression rates in the ablative chamber.

Cryogenic collapse of the pressurant gas was an unexpected and overlooked feature of pressurizing cryogenic rocket propellants. Going into the full system stage test, no mitigation strategies were in place nor was any accounting done during the design phase to mitigate this problem. Upon pressurization, the system immediately saw the helium tank go from 4500 psia to 800 psia, without any other valves opening. Review of video footage showed no indication of a leak and pressure remained steady prior to autosequence start. The hotfire test was still completed to gather some data and demonstrate that the rest of the system was capable of working. To that end it was successful, albeit for a shorter duration. This short duration was the result of a clogged methane filter, likely with frozen water from trapped air in the condenser, that resulted in a long fill time. In order to ensure the test got off, the system was pressurized when it was only partially filled with fuel. Going into the second system level test, diffuser tubes made of 1/4" tube with drilled holes were welded to the fittings that mate the pressurization system to the tanks. These diffusers, pictured previously in Figure 8, and a full propellant tank somewhat mitigated the problems experienced in the first system hotfire. After pressurization of the run tank the system sat at 2200 psia. This meant the system went into blowdown at approximately 3.2 seconds into the burn, rather than at the predicted 7.5 seconds. To further mitigate this pressurization problem the

[†]This value is an estimate

system will be "topped" off with additional helium post pressurization and prior to the helium quick-disconnect being removed from the system.

The design regression rate was nearly an order of magnitude lower than the actual regression rate. This is most likely linked to an error in communication with the vendor when quoting regression rates. Post test images of the chamber show significant melting of the phenolic interior, as opposed to the expected charring. These are presented below in Figure 21.

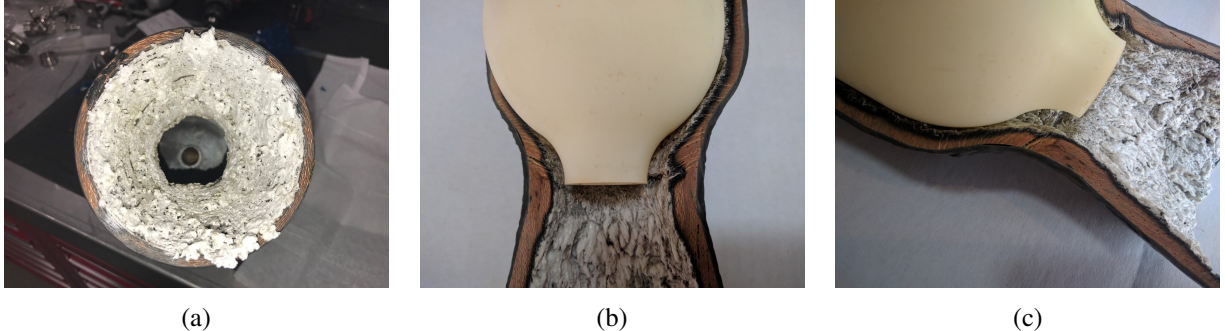


Fig. 21 From left to right: Chamber nozzle, first half of chamber cutaway and mold, and second half of chamber cutaway and mold

The vendor who fabricated the engine predicted a much lower regression rate under the assumption that fuel film cooling would be employed. The injector, as designed, is both fuel centered and lacks a fuel film cooling ring. This point was not effectively communicated to the vendor when discussing possible designs and material selections. While the fuel centered design could result in some amount of oxidizer impinging on the wall and burning with the ablative layer, the lack of cooling is the expected culprit for the results seen in Figure 21. The glass formations indicate that the wall temperature is significantly higher than allowable for the ablative material. While the system could not be changed to allow film cooling, the vendor was able to intersperse Hi-Nicalon Silicon Carbide ply reinforcements to help improve the regression rate. Additional care was also taken during the manufacturing process to reduce the bubbling seen Figure 2.

These tests were important steps in the development of this and future rockets. While the outcome was not desired, the resulting data showed the team where and how to improve the design in order to accomplish flight goals.

VIII. Flight

The team is currently working towards a flight from a local field north of West Lafayette, Indiana. While no date is currently set for the flight, the team is diligently working towards their final milestones in order to be ready for flight before the end of the year.

A. Flight Profile

A flight profile was inputted into MATLAB simulation codes and OpenRocket. Given the current thrust profile and vehicle size, OpenRocket is perfectly reasonable tool for predicting the flight profile.[10] Plots of the predicted flight profile are presented in Figure 22.

The current launch simulations are run for a rocket launched 2° from vertical and from a starting elevation of 600 feet. A 10 m.p.h. wind is assumed to be coming out of the west. The thrust profile was exported directly from the stage test data gathered in the second system hotfire. The predicted altitude is currently just short of 13,000 feet.

The thrust profile, as previously mentioned, was directly imported from the second stage test hotfire. The information for this was previously shown in Tables 3 and 4. The thrust profile selected operated at about half of the design thrust, resulting in a significantly reduced altitude. Since the second stage test, a number of changes were made to procedures and hardware to improve the performance of the system. It is possible that these changes will do very little to improve performance, as seen with the changes completed between the first and second stage test hotfires, but it is recognized that the thrust may be up to 50% higher than seen in the stage test. This was computed by taking the $C_{f,real}$ from stage test one and modifying thrust from stage test two, using the following equation:

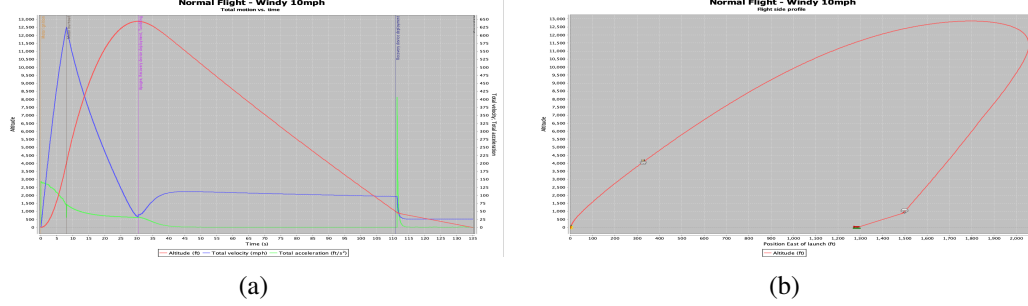


Fig. 22 Plots of (a) altitude, speed, and acceleration vs. time and (b) flight side profile

$$F = \dot{m}C_{real}^*C_{f,real} \rightarrow F_{predicted} = \dot{m}_2C_{real,2}^*C_{f,real,1} \quad (24)$$

To mitigate this issue, the team is planning on discussing this as a risk with the FAA and other launch authorities, including team advisors, during a flight readiness review.

B. Launch Site Selection

The FAR-MARS competition offers a launch site available North of the Mojave Air and Space Port, near the Reaction Research Society's test sites. This launch site, while regularly available and with clearance to launch to the target altitude, is far away from Lafayette, Indiana. This makes logistics more complicated than desired. An alternative launch site, located at a Purdue University research farm, was selected due to previous use by Purdue students in hybrid development work and as a way to minimize cost and risk. Launching locally allows for multiple attempts in the span of days rather than months. The launch site, with circles representing possible landing zones for the rocket, is presented in Figure 23.

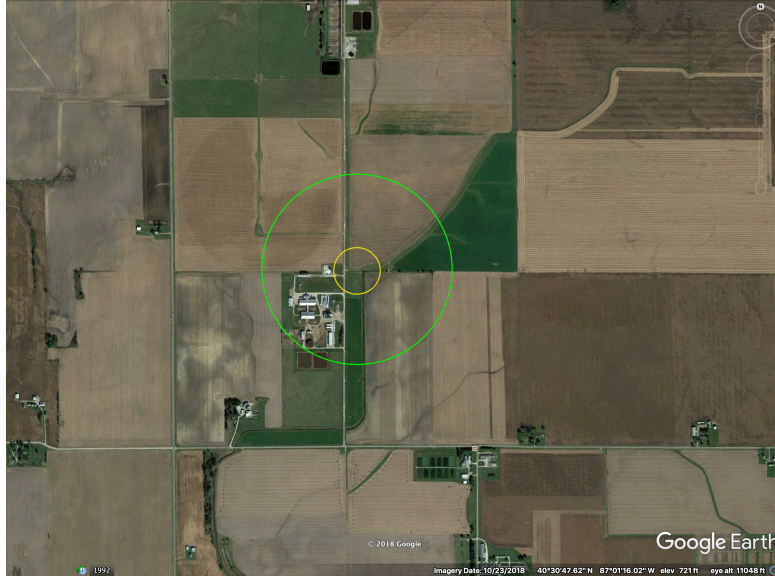


Fig. 23 Launch site with circles representing landing zone with dual deployment (smaller) and single deployment (larger) recovery systems

The circles drawn in Figure 23 are taken directly from the flight profile in Figure 22. The buildings to the south-west are part of the Purdue farm. The direction of launch will be to the north, away from populated areas.

C. Flight Plan

The following is an overview of the flight team and notional flight schedule. This is currently in the early phases of layout and will likely change prior to the team's flight readiness review.

1. Flight Team

The flight team will be assembled similarly to hazardous test teams at Zucrow labs. There will be a flight director, a data system operator, two test operators, and three spotters.

The flight director's role is to coordinate all of the procedures and operations of flight day. They will ensure that all procedural steps are completed and call out all procedures to the data system operator and test operators.

The data system operator manages the console interface for the rocket. They are responsible for monitoring pressures and temperatures and ensuring that the system is safe for the test operators to approach. They are responsible for arming and launching the rocket once the flight director has given the ok to proceed.

The test operators are responsible for ensuring that all manual test operations are completed. They are responsible for connecting rocket propellant to the ground support equipment, managing the supply of consumables, and clearing the area of extraneous personnel when the rocket is filled.

The spotters are stationed at various points of interaction with pedestrian and vehicle traffic. Their job is to maintain eyes on the rocket during launch and also keep an eye out for unauthorized personnel approaching the rocket.

All flight team personnel are equipped with long range radios for communication with the data system operator and the flight director.

2. Notional Schedule

The flight will take place on a weekend. This gives the team plenty of time to work through potential bugs on launch day, avoid conflicts with classes, and allows for a faster recycle on Sunday should the first attempt be scrubbed.

The launch system will be delivered to the launch site on Friday, along with propellants. The trailer will be setup that evening and final checkouts of the electrical systems will take place.

On launch day morning, the rocket will be placed on the launch rail and the launch rail will be raised, as presented in Figure 24.



Fig. 24 Rocket being raised for the first time on July 20th, 2019

Once the rocket is vertical, propellant conditioning can begin. These procedures take between 90 and 180 minutes to execute. Once propellants are ready to be loaded onto the rocket, the system becomes hazardous. All further operations are done remotely. The rocket is loaded, first with oxidizer and then with fuel. Once the propellant tanks are deemed to be full, the propellant quick disconnects are remotely removed from the rocket. At this point, an abort would result in dumping all oxidizer in the rocket through the chamber. Then helium is loaded into the rocket. When the rocket is deemed to be pressurized, the helium fill line is vented and the quick disconnect is actuated. Upon actuation of the final quick disconnect, control of the rocket is handed over to the ground support computer for auto-sequenced launch.

IX. Conclusion

Rockets are hard, but the process of designing, building, and testing this system has provided an amazing learning opportunity for Purdue students of all majors and levels of study. Hundreds of hours spent manufacturing, countless sleepless nights chasing hotfire deadlines, and the investigation of countless unexpected issues in the system have helped the team grow to be strong engineers who do not shy from a challenge. The multiple successful hotfires of this engine design is a standalone achievement, but furthermore this system is another demonstration of the capabilities of Purdue students. The ground work for future projects has been laid for future student design, build, and fly projects in the realm of liquid rocket propulsion systems at Purdue University.

A. Next Steps

The team is working towards flight. Pending flight, and a successful recovery, the team anticipates attempting a second launch within a year of the first. Continuous efforts to improve and rebuild the vehicle offers team members, new and old, an opportunity to become better students and engineers.

1. Improvements

Future design iterations would benefit from looking at the integration of the rocket system. Many components, while purpose built and adequate for their role, do not fit together easily. Assembly of the vehicle can be a tedious and risk process. Aligning wrenches and Allen keys is a major issue and there is a constant risk of cross threading. The fin can and the top of the tank are currently the two most aggravating and risk prone areas on the rocket.

The fin can currently is three separate components spars with fins welded on that attach to the valve mounting ring. They have feet that bolt to the bottom of the tank and the engine. Each fin must be individually attached to the tank while wobbling about, threatening a cross thread if the assembly technician is not diligent. A major spot for improvement would be to mill the fin can out of a single piece of pipe or block and bolt the fins to that piece. A ring style mount, similar to the design of the mid-airframe, would fix the fin can to the rocket and apply thrust to the vehicle. This ring mount would allow the assembly to be slipped over the tank and quickly installed with less risk of damage to the tank hardware.

The top of the tank is also a problematic spot in the design. The methane tank is currently slightly longer than the oxygen tank. This results in a section of pipe sticking past the rocket. The boss seal port was placed too close to the weld location and had to be reported, compromising the weld in the process. This lead to many custom parts being fabricated to avoid having to re-build the tanks. Additionally, with the way the upper airframe is attached, it is impossible to leak check the fitting entering the liquid oxygen tank once the rocket is assembled. It must be torqued prior to mid-airframe assembly, posing some risk to flight operations in case the leak is much larger at pressure than during the lower pressure pneumatic checks completed post assembly.

Additional room for improvement can be found in the lack of significant analysis of the design. While napkin and paper math was often sufficient, there is room to improve the vehicle with better design analysis and more rigorous structural analysis.

2. Future Applications

This project will continue on as a learning tool for new undergraduates and graduate students interested in developing practical hands on skills for designing and testing rocket hardware. While money and interest are two things that are always up in the air with student teams, it is the Team Leadership's hope that new students will be able to find an outlet for their desire to learn more about liquid propulsion by joining this team. While major design work is completed, this vehicle has other applications it could be used for. Peroxide and Triglyme are non-cryogenic hypergolic propellants with a similar volume ratio to oxygen and methane, meaning the vehicle could be quickly re-purposed for flight experiments of experimental engines. Additionally, the tanks can serve as short duration run tanks for other methane and oxygen experiments and already have an interface for load cell integration, as demonstrated by the static fire test stand.

Appendix

Plumbing and Instrumentation Diagrams

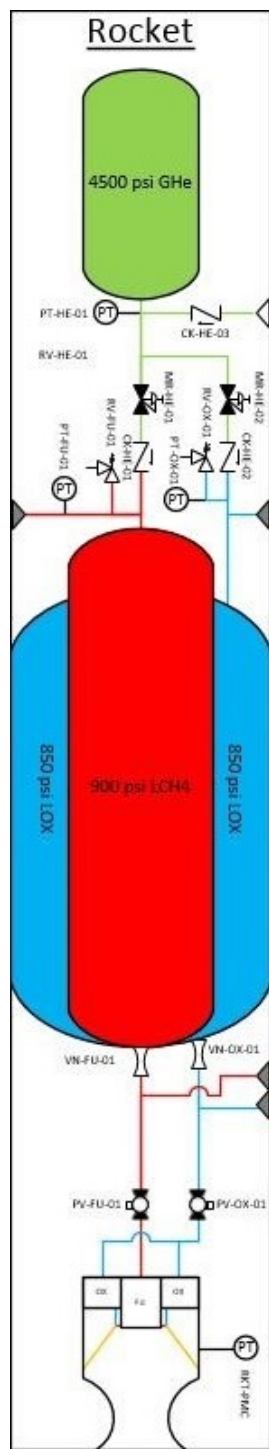
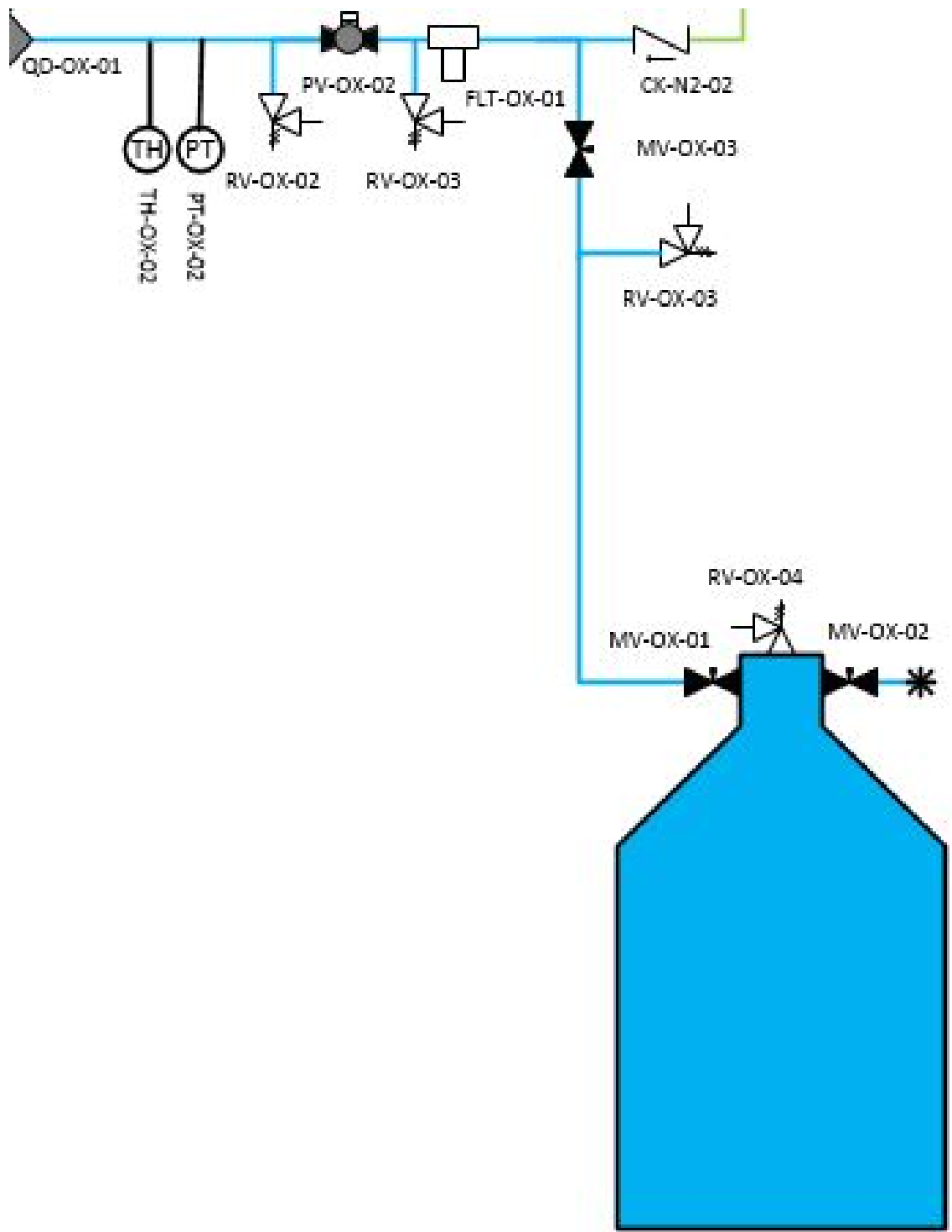


Fig. 25 Rocket P&ID



LOX Dewar

Fig. 26 The P&ID for the liquid oxygen feed system

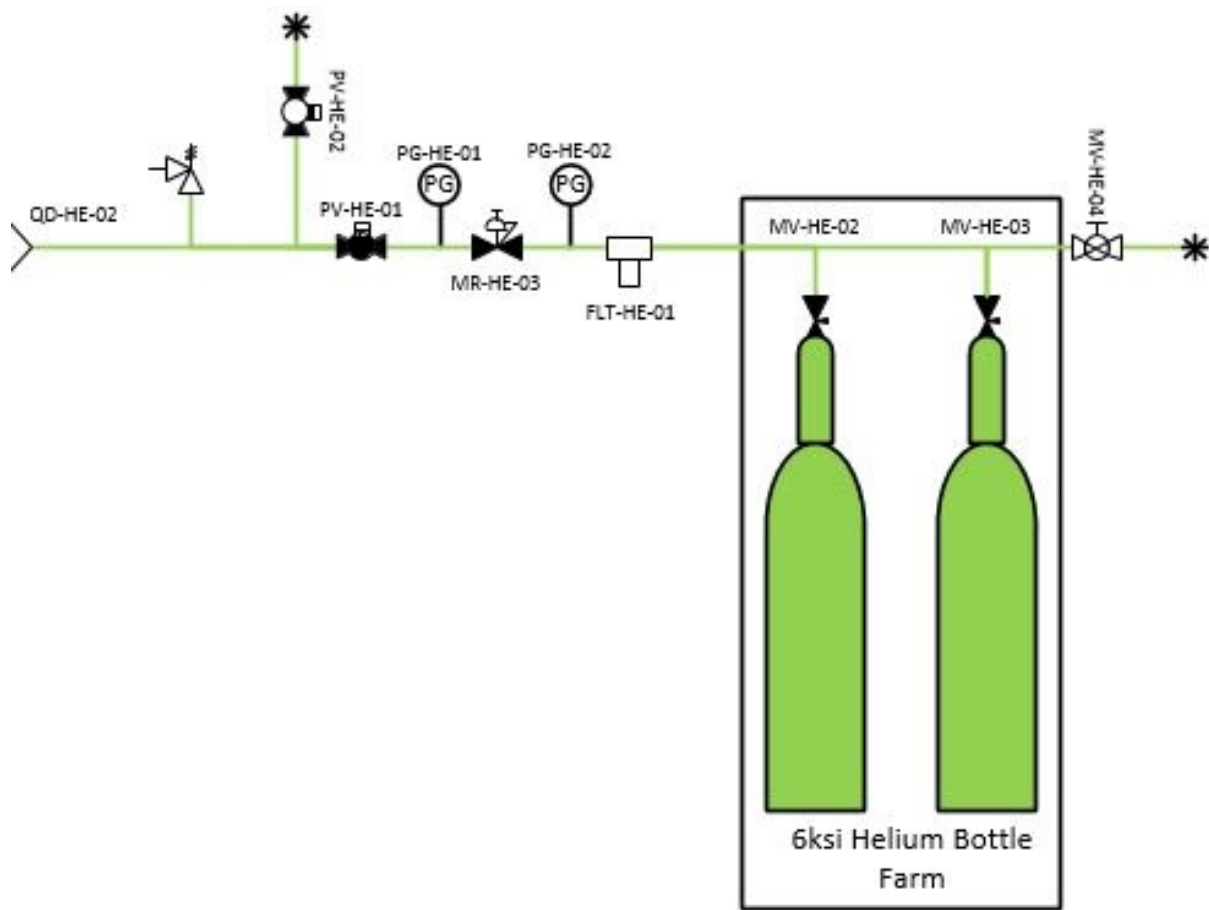


Fig. 27 The P&ID for the methane condenser heat exchanger

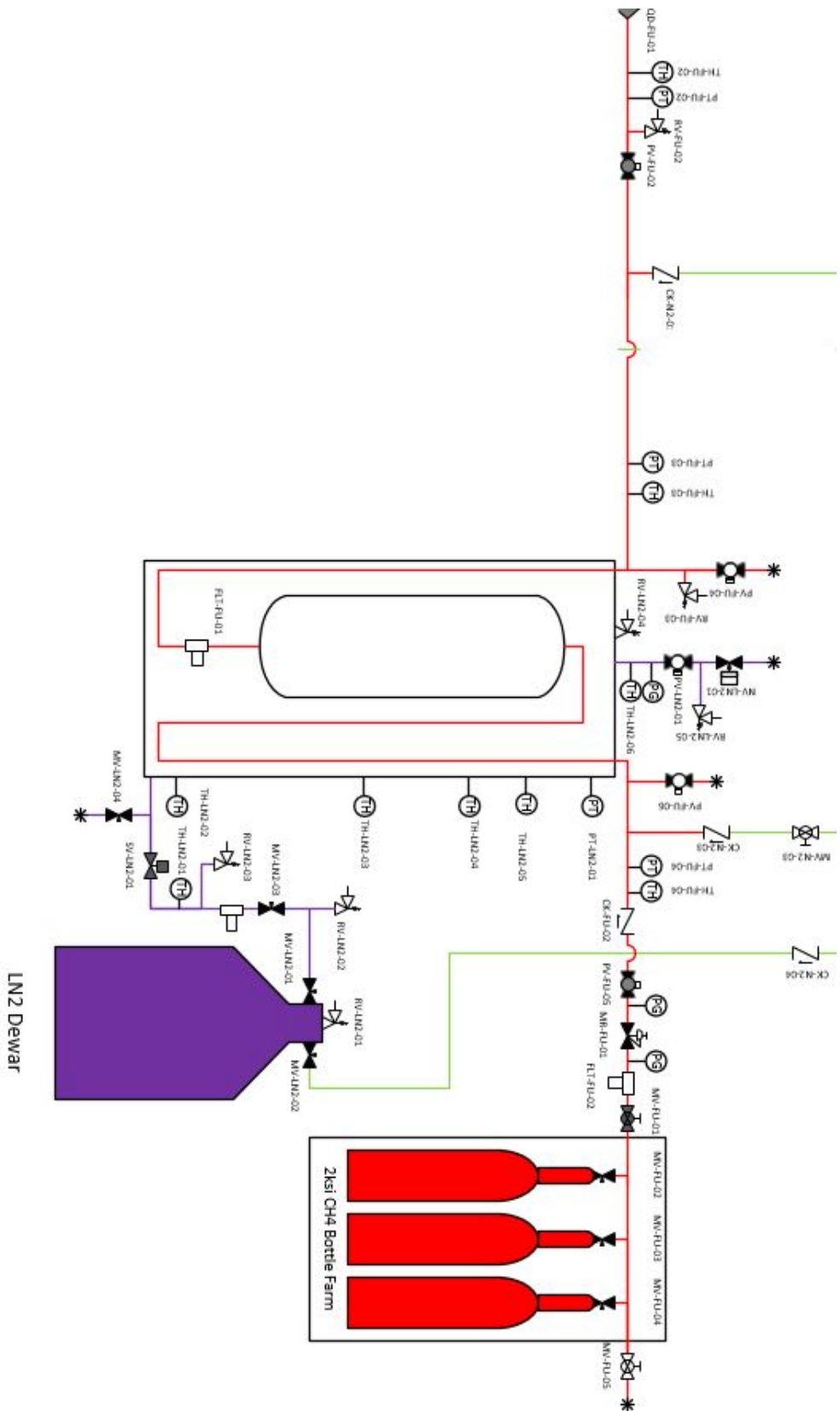


Fig. 28 The P&ID for the methane condenser heat exchanger

SEM Images

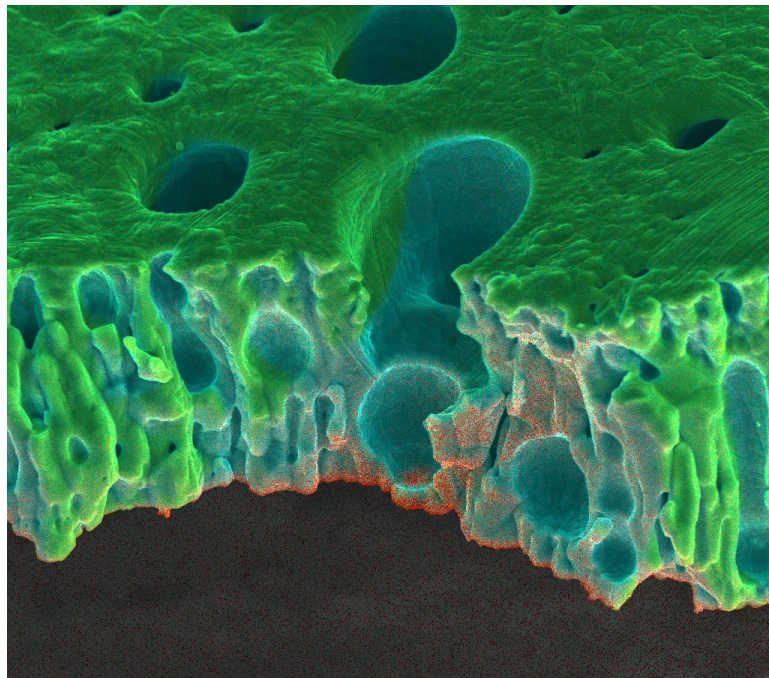


Fig. 29 Composite EDX characterization of injector face build-up, with the spectrum of elemental composition.

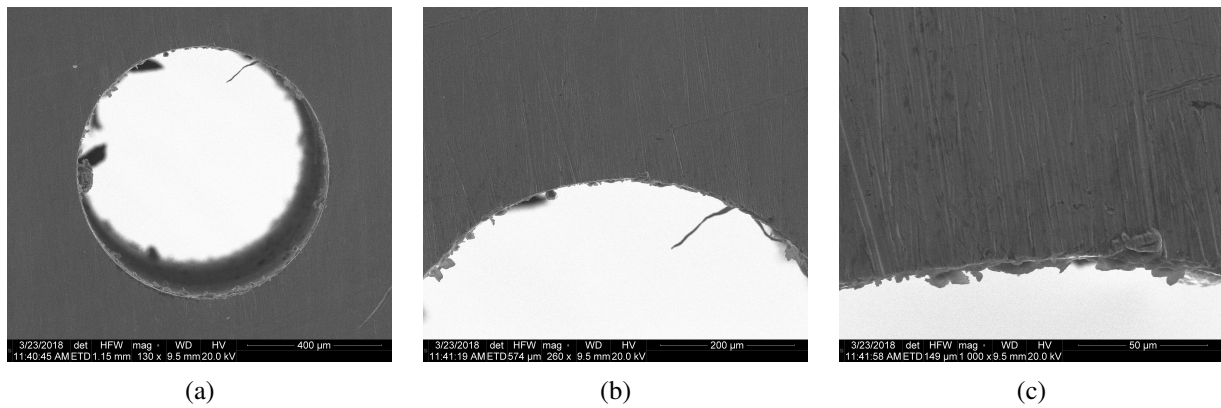


Fig. 30 Baseline-image of pintle hole sample. Clearly identifiable here are the machining marks and artifacts left over by the manufacturing process, which are important for comparison with the post-burn sample. Pictured here are three magnifications: (a) 130x magnification (b) 260x magnification (c) 1000x magnification

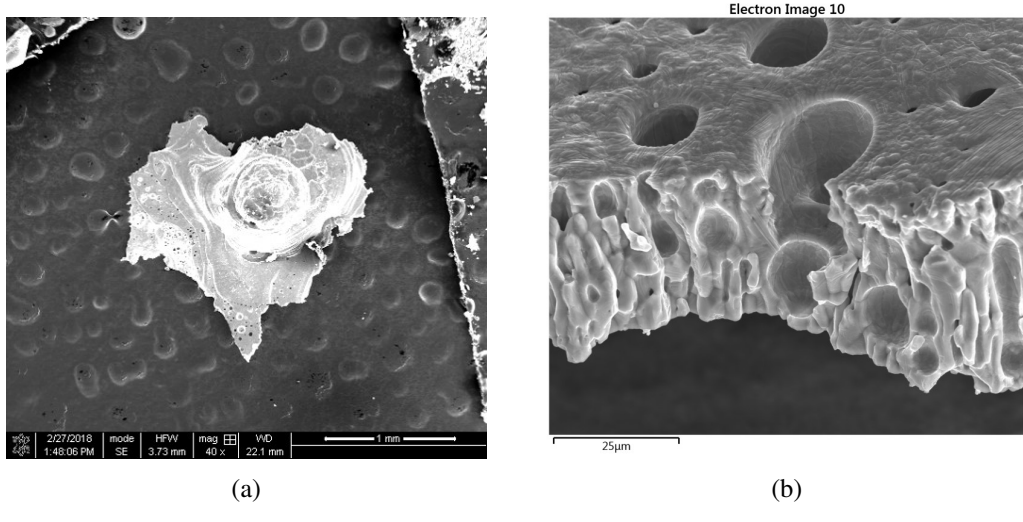


Fig. 31 Topographical images of the sample collected from the combustion-side injector face: (a) is the entire sample, while (b) is one of the sites chosen for EDX imaging and analysis, the results of which are presented in this paper.

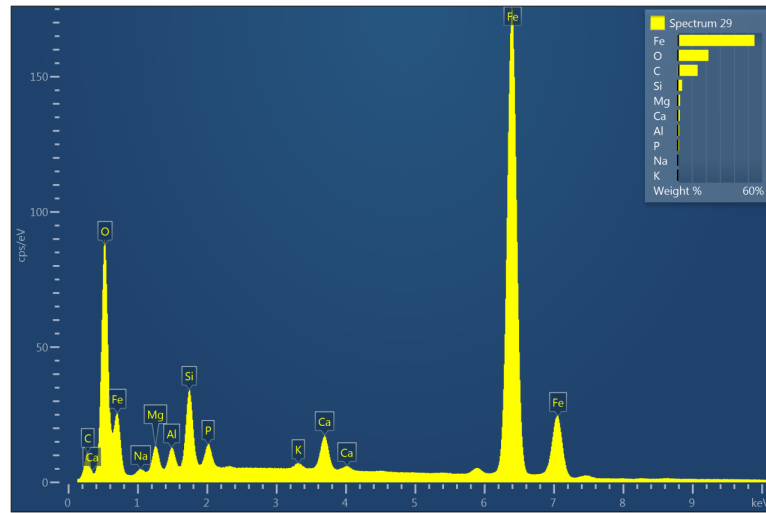


Fig. 32 Spectrum of radiation peaks of injector face build-up. The four elements found in the greatest concentrations are Oxygen, Carbon, Iron, and Silicon (which most likely exists as a result of the o-rings)

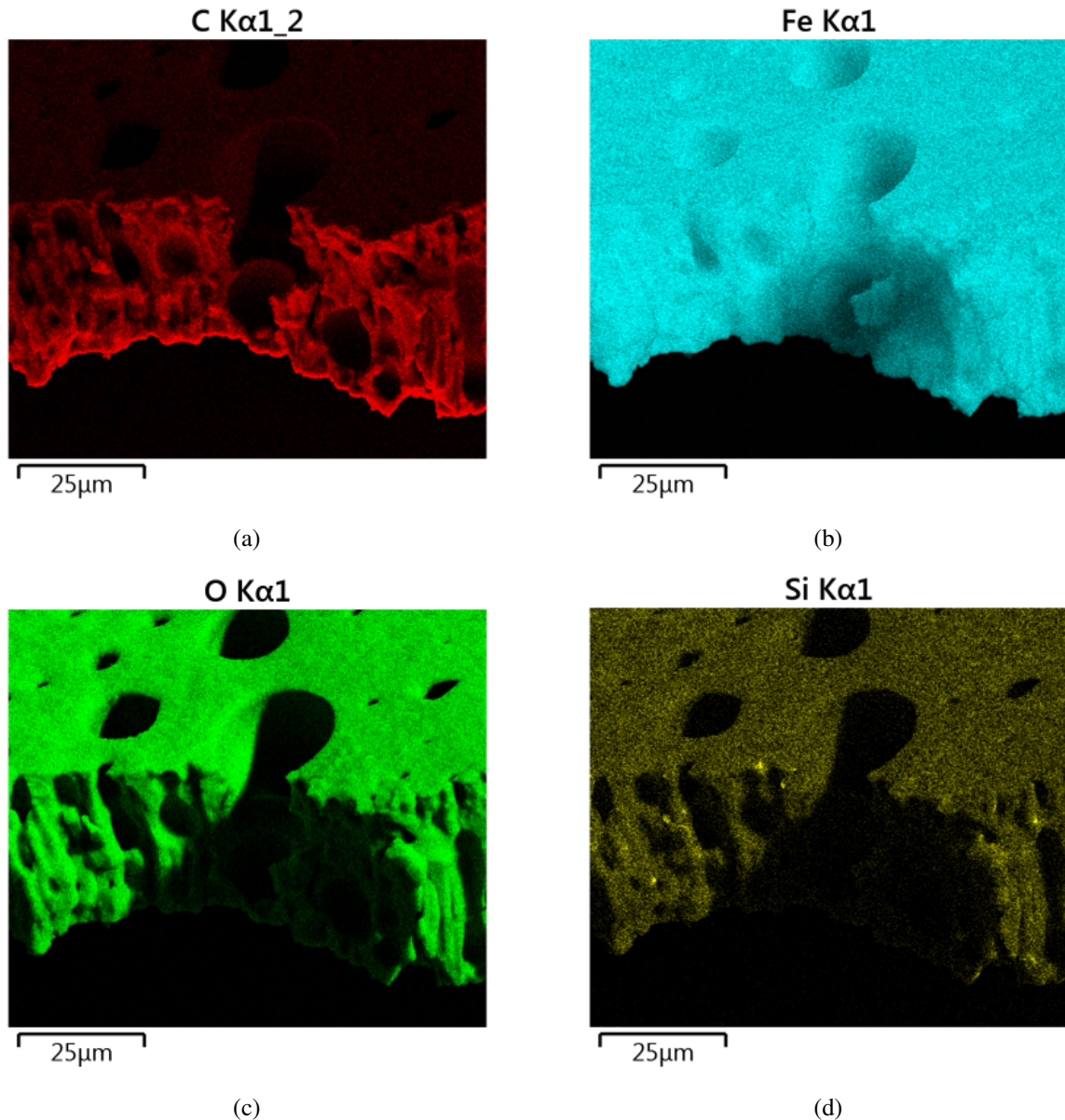


Fig. 33 EDX characterization of injector face build-up, specifically of four most statistically significant individual element concentrations of (a) Carbon (b) Iron (c) Oxygen and (d) Silicon.

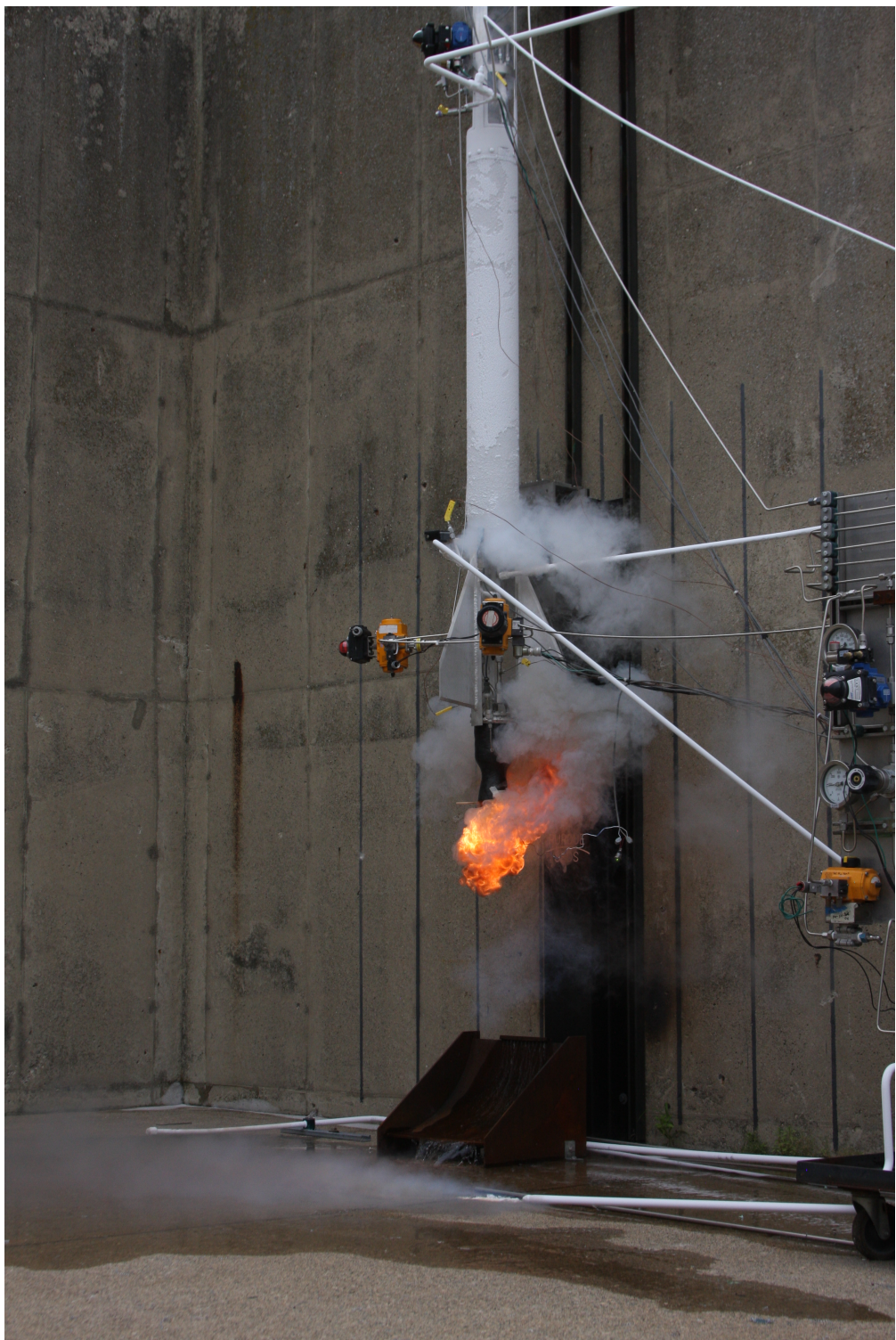


Fig. 34 Igniter start

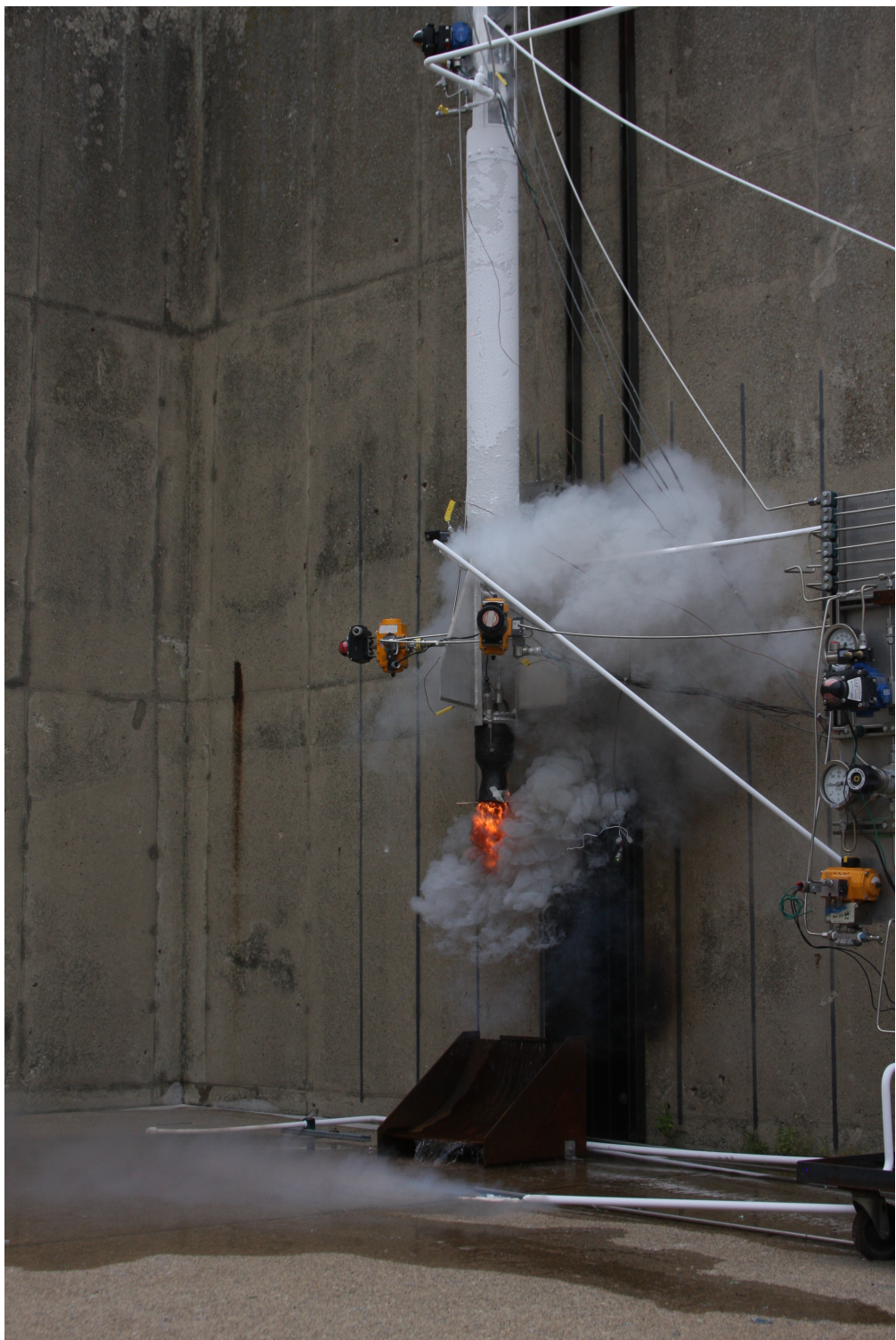


Fig. 35 Rocket propellant valves open, pre-ignition

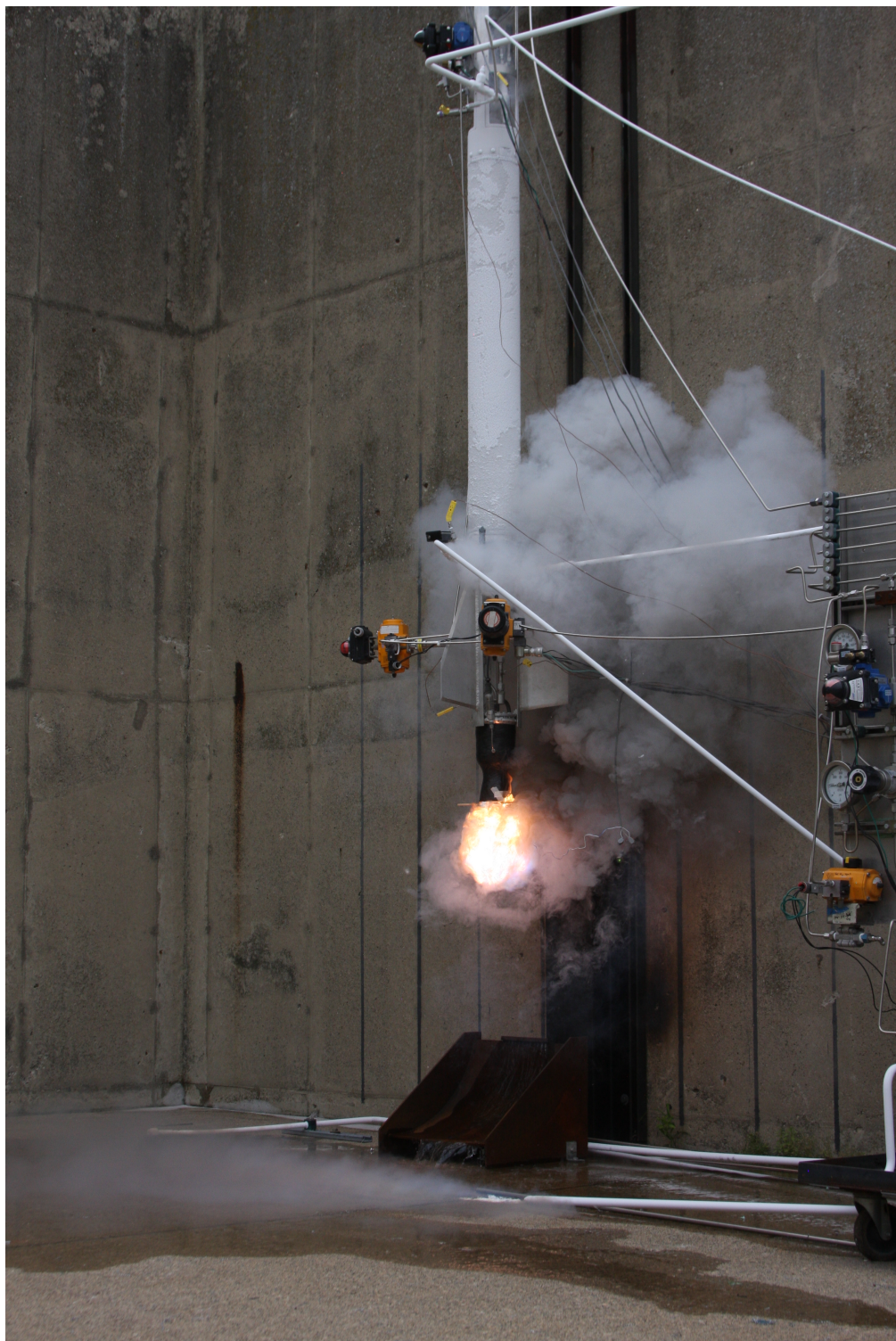


Fig. 36 Rocket engine ignition



Fig. 37 Rocket firing with ice beginning to fall



Fig. 38 Rocket firing with ice falling



Fig. 39 Rocket firing in steady state

Acknowledgments

The authors would like to thank our advisor, Scott Meyer. Your advice and enthusiasm for this project has enabled us to accomplish and learn more than we ever anticipated. Thank you to our reviewer and sanity checker, Dr. Stephen Heister, for your input and advice throughout the process of building this rocket.

Thank you to the volunteers who read and marked up this paper, it's longer and drier than we would have liked but hopefully now its readable.

The team also would like to show incredible thanks to Rob McGuire, Gerald Hahn, the staff and volunteers at Bechtel Innovation and Design Center, and Tole Burnett and all of North Mechanical. Without these people's time and craftsmanship we'd be stuck with lots of metal and no rocket.

Thank you to the Faculty and Staff of Purdue University who we have not yet named. Your insight and willingness to answer our enthusiastic and bottomless well of questions about rocket design have been greatly appreciated.

We are grateful to our sponsors who generously donated hardware to our rocket: Arconic, Norman Filter Co, FlowMaxx Engineering, and Habonim USA.

Computer Aided Design was completed using SolidWorks 2016-2017 and generously provided for the year by Dassault Systems.

Silas Meriam would like to thank all of the graduate students at Zucrow labs who showed interest, enthusiasm, and offered assistance in developing, troubleshooting, and testing this system. He'd also like to thank Ms. Tatumn Vernon for her continued support of his passion for rockets.

Last, but certainly not least, the authors would like to thank every student member who dedicated their time, energy, and knowledge to making this project a success.

References

- [1] Bedard, M., Feldman, T., Rettenmaier, A., and Anderson, W., "Student Design/Build/Test of a Throttleable LOX-LCH₄ Thrust Chamber," *48th AIAA/ASME/SAE/ASEE Joint Propulsion Conference & Exhibit*, AIAA, 2012. doi:10.2514/6.2012-3883, URL <https://arc.aiaa.org/doi/abs/10.2514/6.2012-3883>.
- [2] Tsohas, J., Appel, B., Rettenmaier, A., Walker, M., and D Heister, S., "Development and Launch of the Purdue Hybrid Rocket Technology Demonstrator," 2009. doi:10.2514/6.2009-4842.
- [3] Miklaszewski, E., Dadson, J., Fox, D., Kees, D., Larson, L., Rideout, J., Stevens, J., and L. Pourpoint, T., "Hybrid Rocket Design/Build/Test Course at Purdue University," 2013. doi:10.2514/6.2013-4104.
- [4] "FAR-MARS Launch Contest Rules," , 2017. URL <https://friendsofamateurrocketry.org/launch-contest-rules/>.
- [5] Nilsen, C., Meriam, S., and Meyer, S., "Purdue Liquid Oxygen - Liquid Methane Sounding Rocket," AIAA, 2019.
- [6] "Type K Thermocouple Accuracy," , 2011. URL <https://www.thermocoupleinfo.com/type-k-thermocouple.htm>.
- [7] "Saturation Properties for Nitrogen — Temperature Increments," , 2018. URL https://webbook.nist.gov/cgi/fluid.cgi?TLow=-300&THigh=-100&TInc=5&Applet=on&Digits=5&ID=C7727379&Action=Load&Type=SatP&TUnit=F&PUnit=psia&DUnit=mol%2F1&HUnit=kJ%2Fmol&WUnit=m%2Fs&VisUnit=uPa*s&STUnit=N%2Fm&RefState=DEF.
- [8] "NIST Chemistry WebBook - Methane Phase Change Data," , 2018. URL <https://webbook.nist.gov/cgi/cbook.cgi?ID=C74828&Mask=4#Thermo-Phase>.
- [9] "Data Acquisition & Control," , 2014. URL <https://engineering.purdue.edu/Zucrow/research/lab-infrastructure/data>.
- [10] Niskanen, S., "Development of an Open Source model rocket simulation software," Tech. rep., 2013. URL https://github.com/openrocket/openrocket/releases/download/Development_of_an_Open_Source_model_rocket_simulation-thesis-v20090520/Development_of_an_Open_Source_model_rocket_simulation-thesis-v20090520.pdf.
- [11] Fleeman, E. L., *Tactical missile design*, American Institute of Aeronautics and Astronautics, 2001.
- [12] Sutton, G. P., and Biblarz, O., *Rocket Propulsion Elements*, 9th ed., Wiley, Hoboken, NJ, 2017.
- [13] "MS-01-107 Tubing Data," , 2018. URL <https://www.swagelok.com/downloads/webcatalogs/EN/MS-01-107.PDF>.

- [14] Ghassemi, H., and Fasih, H. F., “Application of small size cavitating venturi as flow controller and flow meter,” *Flow Measurement and Instrumentation*, Vol. 22, No. 5, 2011, pp. 406 – 412. doi:<https://doi.org/10.1016/j.flowmeasinst.2011.05.001>, URL <http://www.sciencedirect.com/science/article/pii/S0955598611000707>.
- [15] Majumdar, A., “Numerical modeling of cavitating venturi – a flow control element of propulsion system,” , 2002.
- [16] Niedzwiedzka, A., and Sobieski, W., “ANALYTICAL ANALYSIS OF CAVITATING FLOW IN VENTURI TUBE ON THE BASIS OF EXPERIMENTAL DATA,” *UWM Technical Sciences*, Vol. 3, No. 19, 2016, p. 215–229. URL http://uwm.edu.pl/wnt/technicalsc/tech_19_3/niedzwiedzka.pdf.
- [17] “Pressure Vessel, Thin Wall Hoop and Longitudinal Stresses,” , 2019. URL https://www.engineersedge.com/material_science/hoop-stress.htm.
- [18] “Euler’s Column Formula,” , 2012. URL https://www.engineeringtoolbox.com/euler-column-formula-d_1813.html.
- [19] Heister, S. D., *Handbook of Atomization and Sprays*, Springer, Boston, MA, 2011, pp. 647–655.